2009

Bending of woody riparian vegetation as a function of hydraulic flow conditions

John O. Goreham
University of Nevada Las Vegas

BENDING OF WOODY RIPARIAN

VEGETATION AS A FUNCTION

OF HYDRAULIC FLOW

CONDITIONS

by

John O. Goreham

Bachelor of Science
New Mexico State University, Las Cruces
2001

A thesis submitted in partial fulfillment
of the requirements for the

Master of Science Degree in Water Resources Management
Department of Water Resource Management
College of Sciences

Graduate College
University of Nevada, Las Vegas
August 2009

ABSTRACT

Bending of Woody Riparian Vegetation as a
Function of Hydraulic Flow Conditions

by

John O. Goreham

Dr. Zhongbo Yu, Examination Committee Chair
Professor of Hydrogeology and Hydrology
University of Nevada, Las Vegas

Vegetation encroachment reduces channel conveyance capacity below design objectives and greatly increases the risk for loss of life and property damage in the case of large flood events. Given minimal knowledge of hydraulic roughness for shrubs and woody vegetation, accurate estimation of channel capacity and water surface elevation is difficult. The ability to predict a tree's bent, reduced height in the presence of flow permits more accurate prediction of hydraulic roughness and water surface elevation.

In this study, field tests were performed to elucidate tree bending properties, which in turn served as input parameters for a numerical algorithm designed to predict tree bending for water velocities likely to be encountered during high flow events. Bending simulations reveal appreciable variability in bent tree heights, likely a manifestation of the extensive variance of plant characteristics and properties inherent in biological specimens. However, no trees were expected to bend to a height lower than approximately 30% of their nonstreamlined height, even in water moving at 2.5 m/s (~ 8 ft/s).

TABLE OF CONTENTS

LIST OF FIGURES

ACKNOWLEDGEMENTS

CHAPTER 1

INTRODUCTION

Problem Statement

Encroachment of vegetation is a severe water resources management problem in

canals, streams, and rivers in the American West. Hydraulic engineers have traditionally

viewed vegetation as part of a maintenance program and therefore, have not accounted

for long-term impacts if left unchecked. As a result of increasing recognition of

ecological benefits, existing flood reduction systems must often be reanalyzed to allow

for vegetation as a source of habitat for various aquatic and riparian species. The

allowance of aquatic and riparian vegetation in older projects results in increased

roughness which affects hydraulic conveyance. The end effect is an increase in hydraulic

roughness (and water surface elevation) for a given flow event. Simply put, vegetation

encroachment reduces channel conveyance capacity below design objectives and greatly

increases the risk for loss of life and property damage in the case of large flood events.

Manning's equation (Equation 1) is instructive in describing the influence of

vegetation encroachment on channel conveyance.

$$Q = \frac{1}{n} A \overset{\downarrow \uparrow}{R}{}^{\frac{2}{3}} S^{\frac{1}{2}} \qquad (1)$$

Manning's equation relates streamflow (volume/time), Q, as a function of hydraulic

roughness, n, channel cross-sectional area, A, hydraulic radius (~ depth, or water surface

elevation), and stream slope, S. The arrows in Equation X indicate the effect of

vegetation encroachment. As the channel becomes inundated with vegetation, hydraulic

1

roughness increases and the effective cross-sectional area decreases. Therefore, if the channel is required to convey a specified Q in order to prevent flooding upstream, the water depth will be required to be greater than it was before vegetation encroachment occurred. It is quite possible that the new water depth will exceed the channel's conveyance capacity, resulting in catastrophic flooding.

The frictional resistance of channel boundaries on flow (i.e. hydraulic roughness or hydraulic resistance) is notoriously difficult to quantify, especially in vegetation, and substantial literature addresses the topic (e.g. Fischenich, 2000; Freeman et al., 2000; Yen, 2002; Baptist et al., 2007; Wilson et al., 2008; Jarvela, 2004; Kouwen et al., 1981; Lopez and Garcia, 2001; Nepf, 1999; Petryk and Bosmaijan, 1975; Wilson et al, 2003). Given minimal knowledge of hydraulic roughness for shrubs and woody vegetation, accurate estimation of channel capacity and water surface elevation is difficult, particularly because hydraulic roughness is not only a function of individual plant characteristics and community composition, but varies with water depth and velocity as plants deform with flow.

Fischenich (2000) proposed the following resistance relations for emergent and submerged vegetation based on the concepts of drag.

$$n = \frac{k_n R^{\frac{1}{6}}}{\left(\dfrac{U}{u_*}\right)\sqrt{g}} \tag{2}$$

$$\text{Where} \quad \frac{U}{u_*} = \begin{cases} \sqrt{\dfrac{2}{A_d C_d R}} & \text{for} \quad \text{Emergent} \\[2em] \dfrac{2.5}{H}\left[\displaystyle\int_0^{h_p} 1.26 h_p^{2} \left(\dfrac{e^{11 C_d A_d \frac{z}{h_p}}}{e^{11 C_d A_d}} \right)^{0.5} dz + \int_{h_p}^{H} \ln\left(\dfrac{\frac{z}{h_p} - 0.95}{0.13 e^{\left(-(C_d A_d - 0.4)\right)^2}} \right) dz \right] & \text{for} \quad \text{Submerged} \end{cases}$$

In Equation 2, h_p represents the effective vegetation height and is dependent on the degree of bending. Therefore, the ability to predict how a plant bends, or more specifically, how its height changes in the presence of flow permits more accurate prediction of hydraulic roughness and water surface elevation.

Vegetation bending will be described hereafter using the terms described below by Equations 3 and 4 where L represents a tree's nonstreamlined height, l refers to its reduced, streamlined height resulting from the drag force experienced due to flowing water, and H_r describes the ratio of height reduction due to bending.

$$h_p = l \tag{3}$$

$$H_r = \frac{l}{L} \tag{4}$$

Objectives

Despite the wealth of research exploring open channel hydraulics, vegetation failure due to wind throw, and vegetation and fluid dynamics, there are, at present, no comprehensive techniques for predicting hydraulic roughness and vegetation bending in open channels.

The purpose of this study is to quantify the height ratios of woody riparian species as a function of water velocity. This was accomplished through a series of field tests to elucidate tree bending properties which in turn serve as input parameters for a numerical algorithm designed to predict tree bending for water velocities likely to be encountered during high flow events. This study focused on key riparian species of the Southwestern United States; however, techniques are generic in nature and analogous data may be collected for additional riparian and terrestrial species. The results will be helpful for supporting bioengineering installation, management of invasive species through washout, investigation of riparian forest stability in high wind events, and assessments of vegetation on flood control levees.

Previous Studies

The relationship between tree resistance to overturning resulting from wind has been investigated considerably for temperate forest trees (Peltola, 2006; James et al., 2006; Gardiner et al., 2008; Lundstrom et al., 2007). Typically these studies have employed "tree pulling" tests to elucidate the applied moment necessary to cause tree uprooting or trunk failure. However, such tests provide no information regarding the changing of tree height and frontal area with fluid flow, and to our knowledge none have addressed woody riparian vegetation. In addition, an extensive body of literature has addressed the impact of fluid flow on plants (e.g. drag force and drag coefficient relationships) (Kane and Smiley, 2006; Freeman et al., 2000; Wilson et al. 2008; Nepf, 1999). However, again, little or no attention is dedicated to the relationship between streamlined vegetation frontal area and height and fluid velocity in these studies.

4

Estimation of the flow-induced drag force on tree crowns is essential for both the prediction of critical wind speed in windthrow models and the understanding of the chronic effects of wind on trees. The classical drag force equation becomes problematic in dealing with porous, flexible vegetation whose frontal areas decrease with increasing wind speed. Rudnicki et al. (2004) and Vollsinger et al. (2005) conducted wind tunnel measurements of tree crown streamlining and drag relationships for coniferous and hardwood species. Both studies report the change in streamlined frontal area as a function of wind velocity, which is of particular interest to this study. Vollsinger et al. (2005) reported at 20 m/s streamlining resulted in the reduction of frontal area to 28% of its still-air value for black cottonwood, 37% for red alder, and 20% for paper birch, while Rudnicki et al. (2004) reported frontal area reductions of 54% for redcedar, 39% for hemlock, and 36% for lodgepole pine for the same wind speed. Both studies revealed drag to be proportional to the product of mass and fluid velocity and also to the product of wind speed squared and wind speed specific frontal area. Neither study reported changes in tree height with wind speed, however.

Theoretical Description of Hydrodynamic-Vegetation Interactions

Vegetation-flow interaction is a complex, highly dynamic process that depends upon many parameters varying from flow steadiness to seasonal condition of the plant. To simplify this multifaceted problem, this study examines vegetation under static loading (steady, uniform flow). Following Peltola (2006), forces acting on vegetation are

coarsely divided into those applied to bend vegetation (fluid drag and gravitational force) and those resisting bending (stem and root-soil resistance) (Figure 1).
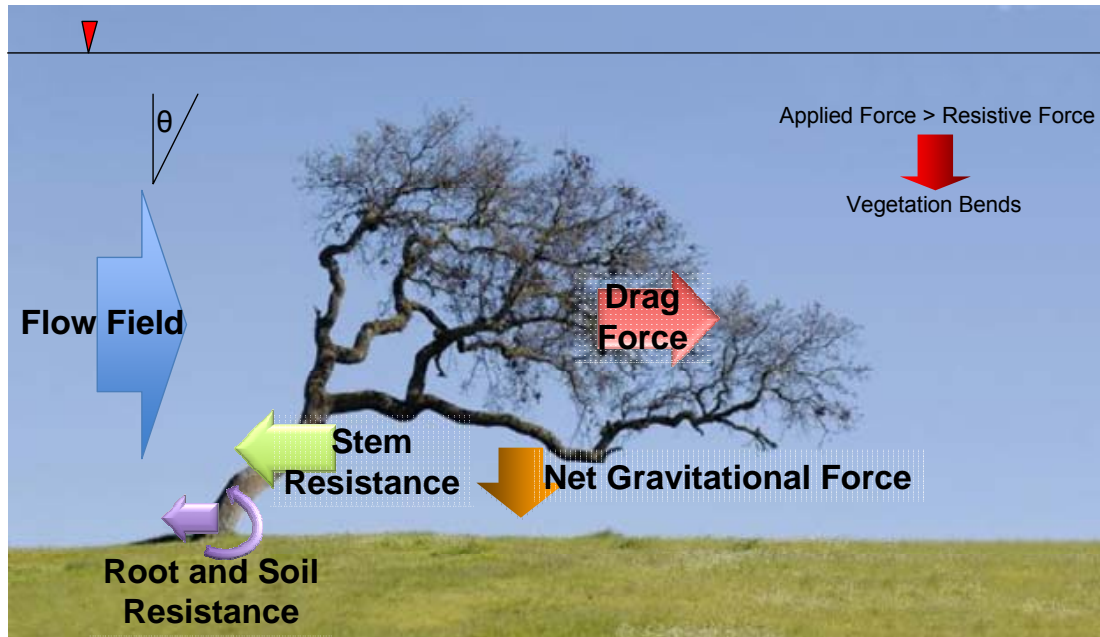
Figure 1. Vegetation-flow static force balance (after Peltola, 2006).

Under steady, uniform flow, the drag induced moment may be expressed functionally as

$$M_{drag} = f\left(h, \rho, \mu, g, C_d(y), A_{veg}(y), V(y)\right) \tag{5}$$

where M_{drag} is the moment induced by hydraulic drag force $\left(F_{drag} = \frac{1}{2}\rho C_d A_{veg} V^2\right)$, y is flow depth, ρ is the fluid density, μ is dynamic viscosity of the fluid, g is gravitational

acceleration, $C_d(y)$ is the drag coefficient, $A_{veg}(y)$ is the area of vegetation exposed to fluid drag, and $V(y)$ is the approach velocity of the fluid.

Net gravitational moment (weight minus buoyancy) varies with the force of gravity acting on the tree as it bends. Thus, net gravitational moment may be summarized as

$$M_{gravity} = f\left(m_{tree}(y,\theta), g, \theta, \gamma_{tree}\right) \tag{6}$$

where $M_{gravity}$ is the moment induced by net gravitational force, m_{tree} is the mass the tree at height y and angle θ, θ is the angle of departure from vertical the tree is bent (Figure 1), and γ_{tree} is the specific gravity of the wood. The total applied moment is expressed as Equation 7.

$$M_{drag} + M_{gravity} = M_{applied} \tag{7}$$

Although two applied forces have been discussed thus far (hydraulic and net gravitational), in riparian environments, net gravitational forces (plant weight – buoyancy) are often insignificant because many riparian plants are young and do not have considerable crown mass and submerged portions provide negligible moment. As such, gravitational forces are neglected in this analysis.

Stem resistance refers to properties of a plant associated with stem bending which are established by examining the material properties. Application of elastic beam theory leads to the following functional form of stem resistive moment for bending.

$$M_{stem} = f\left(y, \theta, d_{tree}(y), h_{tree}, E_y\right) \qquad (8)$$

Where M_{stem} is the moment of stem resistance, y is any distance up the tree, $d_{tree}(y)$ is

stem diameter at y, h_{tree} is total tree height, E_y is modulus of elasticity of the tree at point

y under F_{app} $\left(E_y = \dfrac{F_{app}y}{6I_y \tan(\theta)}\left(3h_{pull} - y\right)\right)$, I_y is moment of inertia at

$y\left(I_y \approx \dfrac{\pi d_{stem,y}^{\,4}}{64}\right)$, F_{app} is the total applied force.

Root-soil resistance is dependent upon the physical characteristics of the site

surrounding the plant and the root characteristics. Site characteristics influencing

resistance to bending include local topography and slope (S_{local}), soil properties such as

texture (e.g. $\%_{coarse}$, $\%_{fine}$), bulk density (ρ_{bd}), and soil moisture (θ_v), and the condition of

scour around the individual tree, which is assumed to impact root-soil resistance through

changes in local topography as a function of flow. In addition to site characteristics,

rooting characteristics are critical to account for root-soil resistance. Tensile strength of

roots (σ_{root}) as well as the combined root-soil tensile strength contributes significantly to

this resistive force (Norris et al., 2008). Additionally, rooting shape and depth are

thought to govern overturning resistance, all of which are highly variable even within a

single species (Coutts, 1983). For the purpose of this discussion, it is assumed that

rooting depth (h_{root}) alone is the driving factor. As such, root-soil resistive moment

(M_{root}) may be expressed functionally as:

$$M_{uproot} = f\left(y, S_{local}, \%_{fine}, \%_{coarse}, \rho_{bd}, \theta_v, \sigma_{root}, h_{root}\right) \qquad (9)$$

8

CHAPTER 2

METHODS

Site Selection

In order to address the research objectives, field sites were chosen throughout the Southwestern United States with a focus on selecting sites with similar riparian community composition but a sufficiently large array of other environmental conditions. The environmental variables deemed important, based on our conceptual understanding of the problem described above, included sediment characteristics, species composition, depth to groundwater, and size and density of trees. Based on vegetation surveys conducted throughout the region and availability of hydraulic drag characteristics, the following taxonomic groups were deemed frequent and relevant for targeting in the experimental design: willows, cottonwoods, and salt cedars.

Securing access to field sites was a significant challenge due to the environmental concerns surrounding the removal of trees in a region of the country in which riparian vegetation is at a premium. The project team compiled a list of more than a dozen potential sites and contacted the relevant land-owners and managers.

The first testing site was located in the San Luis Rey River (SLR) in Oceanside, California. The SLR has dense vegetation throughout the lower 12 km of the river including willows, cottonwoods, and to a lesser extent, salt cedars. The study site is within a USACE flood damage reduction project and in most cases the vegetation covers the entire channel bed. The first test site in the SLR was located approximately 0.75 km upstream of Foussat Road. The site had a high degree of variability in both vegetation and environmental characteristics including soil types, soil moisture content, and depth to

groundwater. A defined low flow channel existed at Site 1 but no surface water was present during testing. However, the soil moisture content was nearly saturated at several of the test locations. The second site in the SLR was located approximately 0.25 km downstream from Bennett Road. Flowing water was present within the study reach at Site 2 a horizontal distance of approximately 20 m and vertical distance of approximately 0.5 m from the test locations. The locations of Sites 1 and 2 in the SLR are shown on a Google Earth Map in Figure 2. Testing was conducted in the SLR from September 16th to the 18th, 2008.
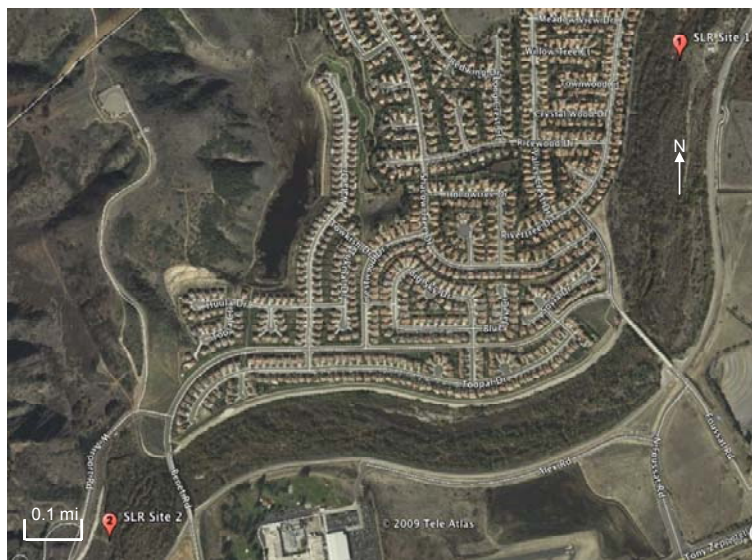
Figure 2. Data collection Sites 1 and 2 in the San Luis Rey in Oceanside, CA.

The second round of tests were conducted at the Las Vegas Wash (the Wash) on salt cedars based on permission from the Las Vegas Wash Coordination Committee (see Figure 3). Two test sites were investigated at the Wash, the first located at 36°06'59.2"N and 115°01'46.73"W near E Rochelle Avenue, and the second at 36°05'28.61"N and

114°59'46.80"W, approximately 4 km downstream from Site 1 and approximately 1 km above Pabco Weir. Testing was conducted during September 30 to October 1, 2008.

Figure 3 is a Google Earth map showing the locations of both Wash sites. Site 1 was located within the active floodplain and experienced minor flooding prior to testing. The variable elevations available at Site 1, due to the presence of floodplain terraces, allowed for pull tests over a range of depths to groundwater. Site 2 was located on a perched bank, approximately 10 m above the water surface elevation in the Wash.

The third field site was located on the Rio Grande (RG) in Albuquerque, NM (see Figure 4). Site 1 was located approximately 1.5 km upstream from the I-25 bridge and Site 2 was located an additional 400 m upstream from Site 1. Site 1 was located on the west side of the RG along the river side of the flood control levee (approximately 50 from the River). Site 2 was also on the west side of the river but was located on the non-river side of the levee. Testing was conducted on December 19th and 20th, 2008.
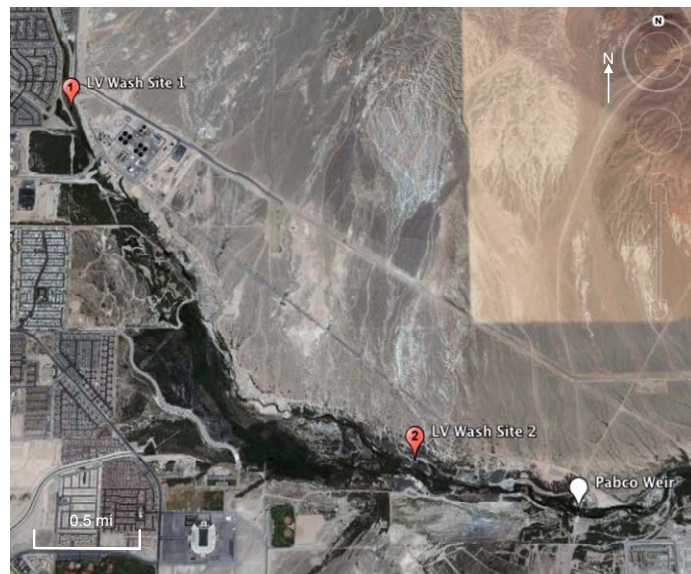
Figure 3. Las Vegas Wash test Sites 1 and 2 near Las Vegas, NV.

Figure 4. Rio Grande Sites 1 and 2 in Albuquerque, NM.

Field Experiments

In order to predict vegetation bending as a function of hydraulic flow conditions, the tree's modulus of elasticity, E (N/m), and second moment of area, I (m^4), must be known. Tree pulling tests were conducted to elucidate E values for target vegetation. Vegetation bending was induced by exerting force via an anchored tree pulling apparatus (Figures 5 and 6).
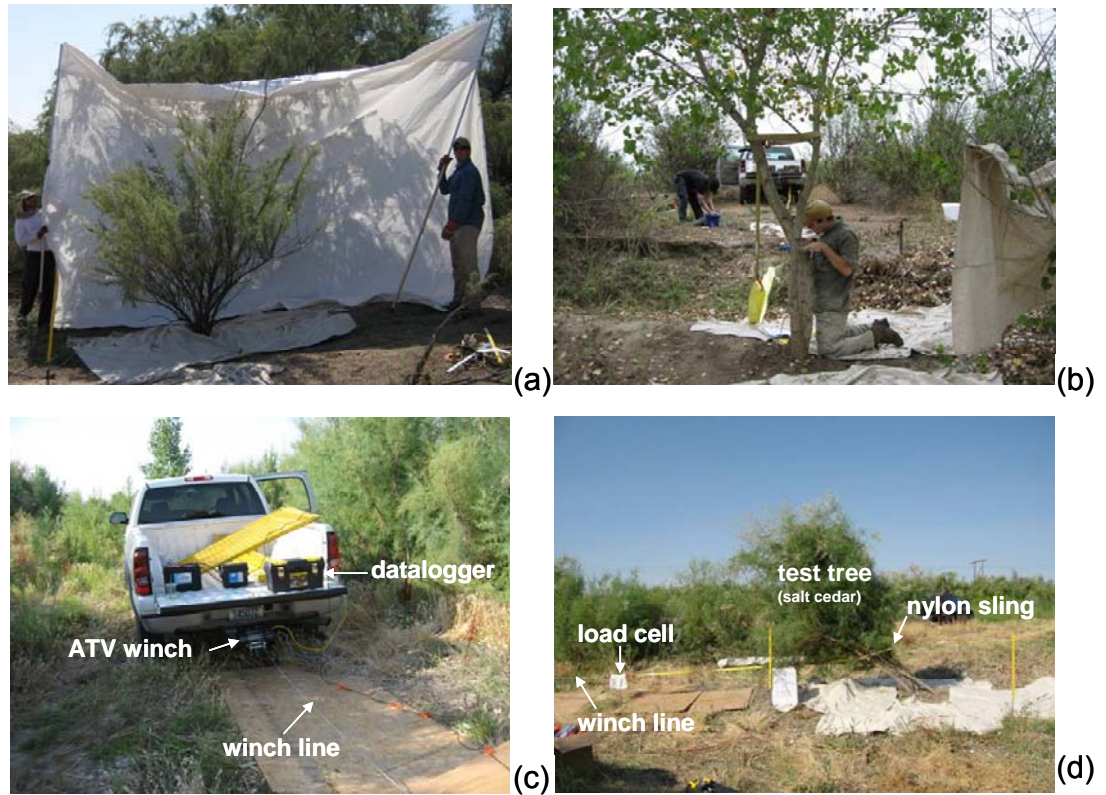
Figure 5. Tree pulling experimental setup: (a) Collection of nonstreamlined frontal area, A0, (b) Description of trunk diameter, (c) Force application, (d) Attachment to tree.
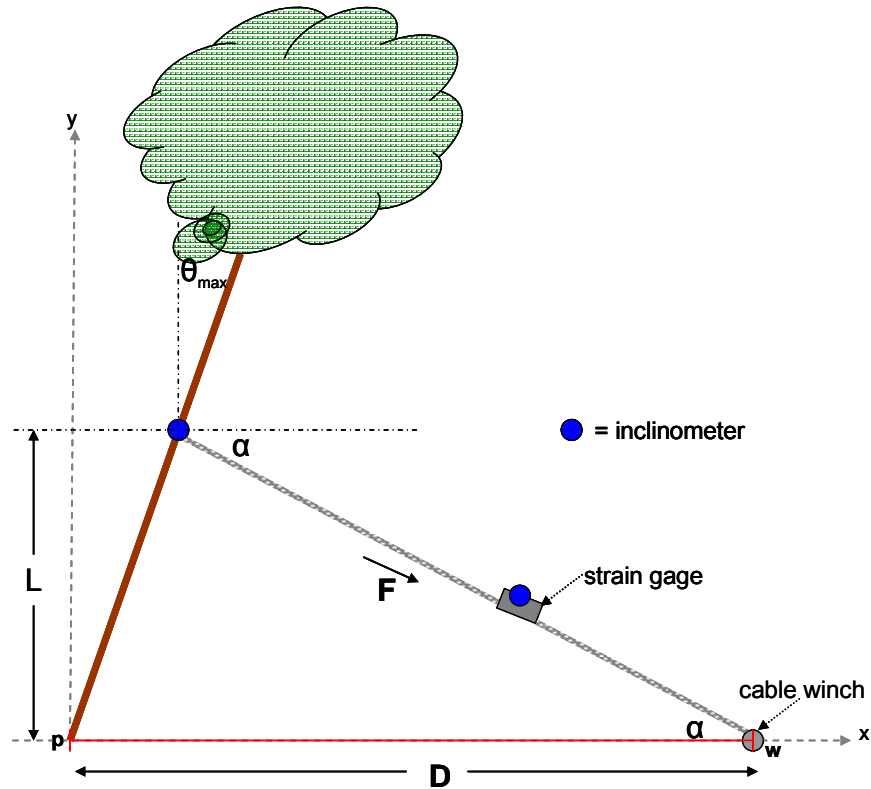
Figure 6. Generalized tree pulling setup: α, pull angle; θmax, maximum slope of trunk of length L, occurring at the point of winch line attachment; F, pull force; D, horizontal distance between pivot point, p, and winching point, w.

Testing protocols were adapted to riparian environments from methods used in tree stability testing in silvicultural forests (Nicoll et al., 2006). For ease of transport, the experimental design used a ¾-ton truck and mounted ATV winch for applying the force. A strain gage was used to measure the applied force and digital inclinometers collected pulling and bending angles (α and θ, respectively). Force was applied at approximately one-fourth to one-third of total tree height for all specimens in order to provide consistent scaling between tests. Profile videography of each tree was recorded throughout the test. Prior to each test, a suite of parameters was collected, including: individual vegetation characterization, site properties, and test conditions (height of pull point and winch, etc.).

Figure 7 features a typical recorded time series for a pull test describing the bending response of the tree as a moment resulting from the pull force is applied. As the pull test progresses, the tree bending angle decreases until the tree is pulled flat to the ground at approximately 16:43:41, at which point the pull force increases considerably as an attempt is made to pull the tree completely from the ground.
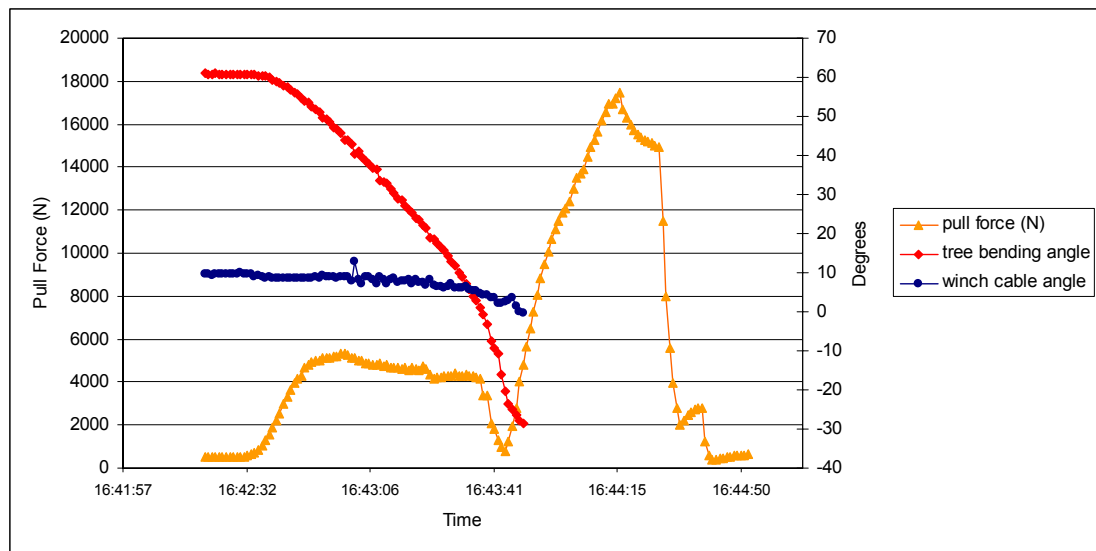
Figure 7. Tree pulling test time series.

Elastic beam theory, in conjunction with data obtained from pull tests, permits computation of E. In employing elastic beam theory for the calculation of E, the following simplifying assumptions were made:

1. The portion of the tree trunk of interest for the computation of E is limited to that from the ground to the point of attachment of the winch line. The trunk is assumed to be elastic, homogenous material.

2. The trunk is assumed to be a cylindrical cantilever beam of uniform diameter from its base to the attachment point of the winching line. For trees with a single main trunk, typically the diameter of this beam was smaller at the attachment point than at the base. For purposes of simplification, the beam's representative diameter is computed as the average of these two diameters. Salt cedars often exhibited multiple stems at both the base and attachment point. For these cases, the cross sectional areas for the basal stems were summed and then an equivalent diameter was calculated. This was repeated similarly for multiple-stemmed attachment points. As with single trunk trees, these two diameters were then averaged to give a single representative diameter for the beam.

3. Deformation is caused by bending rather than shear.

The generalized, small deflection of an elastic, homogenous cantilever resulting from the application of a force, F, at its end is depicted in Figure 8 below. Note that for small deflections, it is implied that: (1) no vertical deflection occurs; (2) deflection occurs only horizontally; and (3) force is applied horizontally.

Elastic beam theory for deflections of elastic, homogenous material is described by Equation 10 (Hibbeler, 2009).

$$\frac{\dfrac{d^2x}{dy^2}}{\left[1+\left(\dfrac{dx}{dy}\right)^2\right]^{\frac{3}{2}}}=\frac{M}{EI} \tag{10}$$
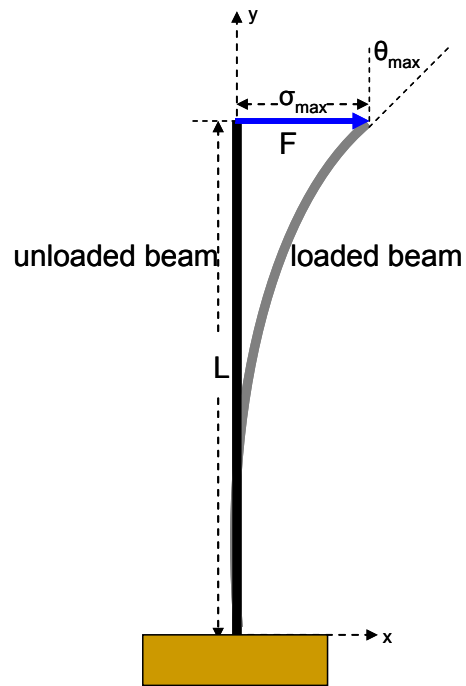
Figure 8. Small deflection of an elastic, homogenous cantilever.

This equation represents a nonlinear second-order differential equation. Solution of Equation 10 gives the exact shape of the elastic curve, x = f(y), where M is the internal bending moment in the beam at y. As we are dealing with small deflections, i.e., the slope of the elastic curve is small, an important simplification can be made to Equation 10. It can be assumed dx/dy is approximately zero. Consequently its square is negligible compared to unity and Equation 10 reduces to the following linear differential equation

$$\frac{d^2 x}{dy^2} = \frac{M}{EI} \tag{11}$$

Integration of Equation 11 gives

$$\theta_{max} = \frac{FL^2}{2EI} \quad \text{at x=L} \tag{12}$$

where θ_{max} is the maximum slope of the beam, F is the force applied horizontally at the end of the beam, and L is the beam length (See Figure 8).

F and θ_{max} were provided by the strain gage and the inclinometer positioned at the attachment point on the tree, respectively, and L was measured before each test. The tree's second moment of area, I, is computed using the representative diameter described earlier. The equation for the second moment of area for a cylindrical cross section is given by

$$I = \frac{\pi}{64} D^4 \tag{13}$$

Solving Equation 13 for E gives

$$E = \frac{FL^2}{2I\theta_{max}} \quad \text{at x=L} \tag{14}$$

As described earlier with regard to Figure 8, elastic beam theory implies horizontal application of force, P. During field tests the actual angle of force application with

respect to horizontal varied, but as α typically was very small (<5 degrees), violation of the assumption was negligible.

Estimating Hydraulic Drag Forces and Tree Bending Predictions

In the discussion to follow regarding tree bending due to hydraulic drag forces, the following general assumptions are made:

1. Vegetation is fully submerged in flowing water.

2. The tree for which bending is to be predicted is the sole occupant of the channel.

3. No scouring of channel bed material occurs.

4. The vertical water velocity profile is uniform.

Prediction of vegetation bending as a function of hydraulic flow conditions requires an estimate of the drag force, F_d, exerted on the object for a given water velocity. The drag force equation is given by

$$F_d = \frac{\rho C_D A_f V^2}{2} \tag{15}$$

where ρ is the density of the fluid, C_d is the drag coefficient, A_f is the streamlined frontal area of the tree lying in a plane perpendicular to the direction of flow, and V is water velocity. Calculation of F_d requires an estimation of A_f. Studies investigating changes in A_f as a function of fluid velocity are scant. However, one study in particular is pertinent to this investigation. Vollsinger et al. (2005) conducted wind tunnel measurements of tree crown streamlining for several hardwood species common to northwestern North

America. Their study described the relationship of frontal area ratio, A_r, (streamlined frontal area / nonstreamlined frontal area) of unpruned crowns of black cottonwood (AC), red alder (DR), paper birch (EP), trembling aspen (AT) and bigleaf maple (MB) digitized from video images at wind speeds (U) from 0 to 20 m/s (See Figure 9).
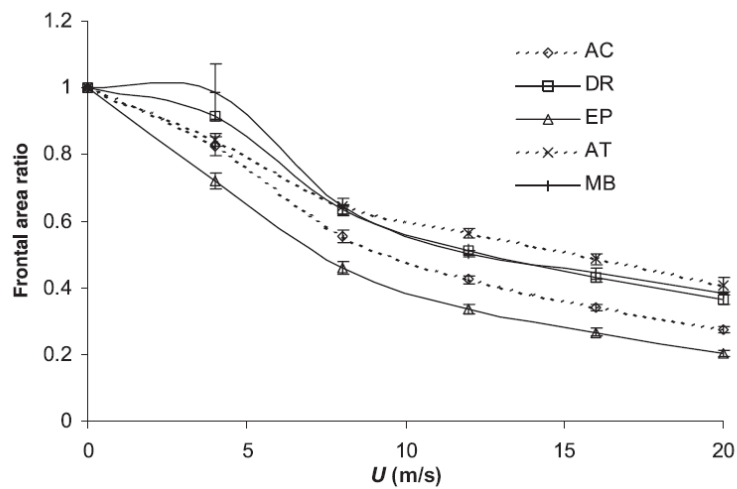
Figure 9. Frontal area ratio of unpruned crowns of black cottonwood (AC), red alder (DR), paper birch (EP), trembling aspen (AT) and bigleaf maple (MB) as a function of wind speed (from Vollsinger et al. 2005).

A request made to the authors for access to their data was unanswered. Consequently, Figure 9 was digitized in order to develop a function describing the relationship between A_r and water velocity, V_{water}. Transformation of the x-axis in Figure 9 into V_{water} is of greater utility for this study and follows from the definition of the Reynold's number

$$\text{Re} = \frac{\rho V D}{\mu} \tag{16}$$

where ρ is fluid density, V is fluid velocity, D is the diameter of the object, and μ is the fluid's dynamic viscosity. The relationship described by Equation 17 follows, and can be solved for V_{water}.

$$\frac{\rho_{air}V_{air}D}{\mu_{air}} = \frac{\rho_{water}V_{water}D}{\mu_{water}} \tag{17}$$

The relationship describing A_r and V_{water} derived from Vollsinger et al.'s (2005) findings is featured in Figure 10. Note that Figure 10 also includes the plot of the average A_r for the five species included in the Vollsinger et al. (2005) study. In Figure 11, an exponential regression (Equation 18) is fit to the average A_r data points. The choice to use an exponential regression, rather than a linear one, was guided by the former's ability to more accurately capture the physical phenomenon of vegetation streamlining in which a relatively large degree of streamlining occurs at low velocities (<1.0 m/s) and then asymptotically approaches maximum streamlining at higher velocities (>1.5 m/s).

$$A_r = 1.0017e^{-0.843V_{water}} \tag{18}$$
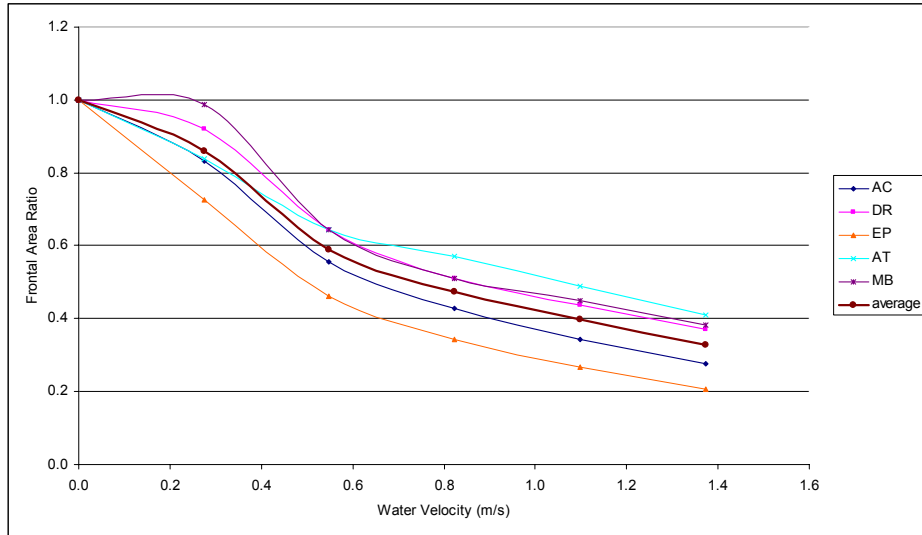
Figure 10. Frontal area ratio of unpruned crowns of black cottonwood (AC), red alder (DR), paper birch (EP), trembling aspen (AT) and bigleaf maple (MB) as a function of water velocity (modified from Vollsinger, 2005).
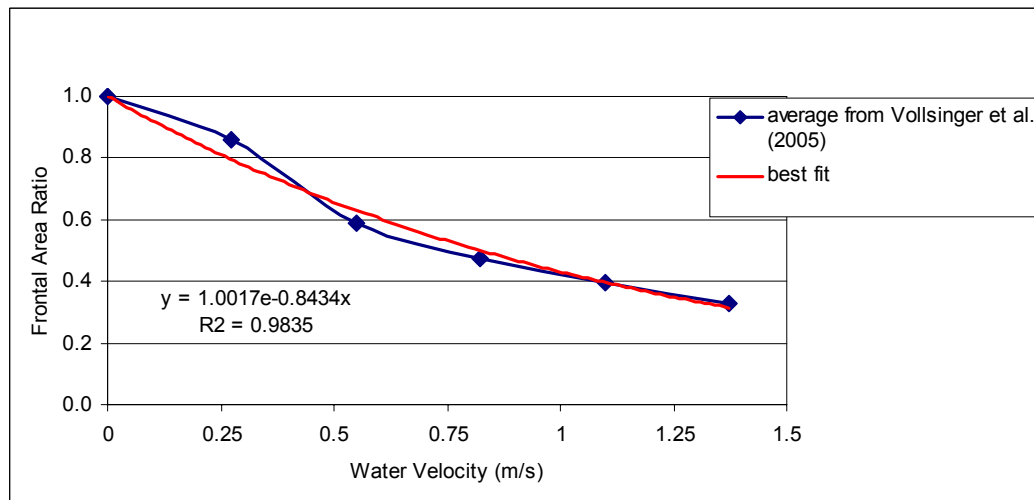
Figure 11. Exponential regression describing frontal area ratio vs. water velocity for water velocities $\leq$ 1.37 m/s.

It is recognized that the true A_r value for a particular tree for a given velocity will deviate from the value predicted by the best fit equation. For example, Vollsinger et al. (2005) noted at a wind speed of 20 m/s (1.37 m/s in water) the frontal area reduction of

alder was half that of birch. For this reason, the impact of A_r variability on predicted

bending is investigated later in this thesis through a sensitivity analysis. However, in the

absence of existing data for the target species in this study, Equation 18 provides a

reasonable estimate for the prediction of A_r as a function of V_{water} for $V_{water} \leq 1.37$ m/s.

In a flume study designed to elucidate hydraulic roughness values for shrubs and

other flexible vegetation, Freeman et al. (2000) observed maximum streamlining of

vegetation at a water velocity of about 1.2 m/s, where the term "maximum streamlining"

refers to no significant decrease in A_r with increasing velocity. Figure 12 describes this

phenomenon.
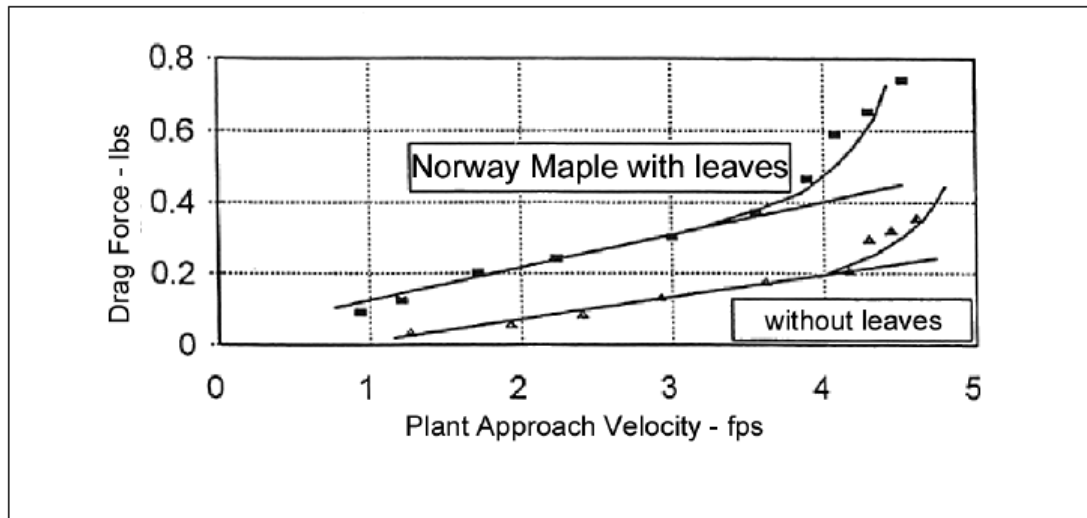
Figure 12. Drag force vs. water velocity for Norway Maple trees with and without
leaves (from Freeman et al. 2000).

The drag force varies almost linearly with velocity for velocities less than about 1.2

m/s (4 ft/s), indicating the occurrence of streamlining. If plant resistance were constant

with increasing velocity, the drag force equation indicates a plot of drag force versus

water velocity would appear as an exponentially increasing function. The graph in Figure 12 adopts the expected exponentially increasing form around 1.2 m/s (4 ft/s), indicating the occurrence of maximum streamlining.

This study investigates vegetation bending during high flow events, during which water velocities are likely to exceed 1.37 m/s, perhaps even as great as 2.5 m/s. To our knowledge, no studies have investigated streamlined vegetation frontal area behavior for water velocities exceeding 1.37 m/s.

As stated previously, Freeman et al. (2000) observed maximum streamlining around 1.2 m/s, while Vollsinger et al.'s (2005) study suggests considerable, although not maximum, streamlining at a wind speed of 20 m/s ($V_{water} = 1.37$ m/s) (see Figure 13).

In the absence of existing data specific to vegetation and water velocities of interest in this study, a reasonable, generalizable assumption regarding frontal area ratios as a function of water velocity for velocities exceeding those examined in previous work (i.e., those greater than 1.37 m/s) must be made. In light of these limitations, an attempt to "book end" the A_r versus V_{water} relationship for this study's target species is made. This is done by exploring two possibilities, guided by the following two assumptions:

1. "Maximum streamlining" assumption: Maximum streamlining occurs at 1.37 m/s (see Figure 14), i.e., $A_r = 0.329$ for $V_{water} > 1.37$ m/s.

2. "Best fit" assumption: A_r values will be extrapolated beyond $V_{water} > 1.37$ m/s with the aid of Equation 7. That is, $A_r = 1.0017e^{-0.843V_{water}}$ for $V_{water} > 1.37$ m/s (see Figure 14).
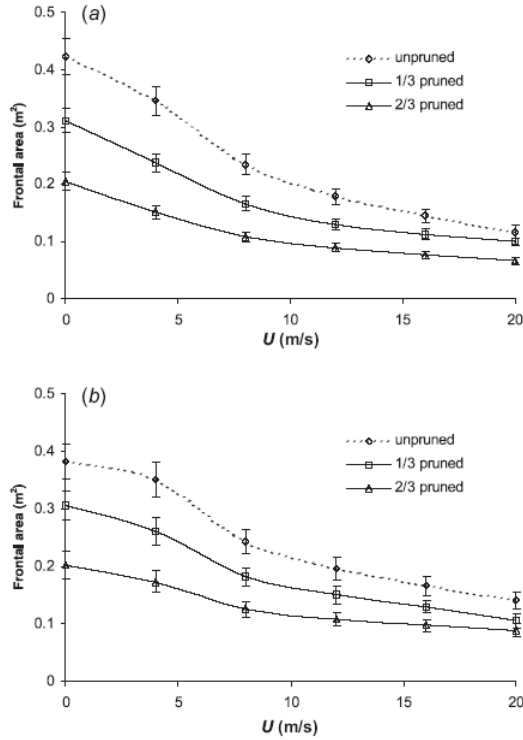
Figure 13. (a) Frontal area (m2) for black cottonwood and (b) red alder crowns (from Vollsinger et al. 2005).
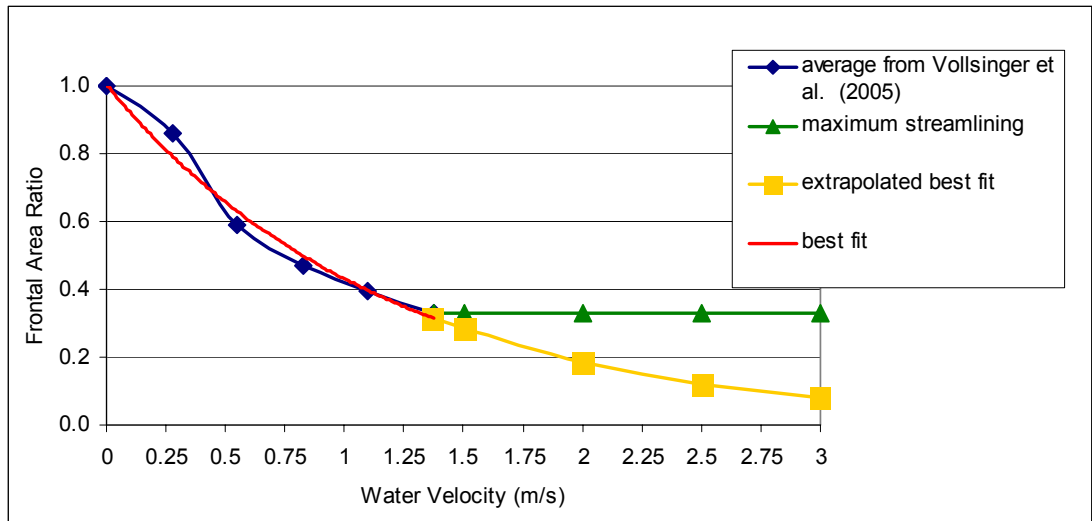
Figure 14. Frontal area ratio versus water velocity. For Vwater > 1.37 m/s, Ar values are extrapolated according to the "best fit" and "maximum streamlining" assumptions.

Because the moduli of elasticity and second moment of areas for the vegetation featured in both Freeman et al. (2000) and Vollsinger et al.'s (2005) studies and our target vegetation do not differ appreciably, it is reasonable to posit that, in general, the streamlining behavior for the vegetation examined in this study for velocities exceeding 1.37 m/s lies somewhere in the area bound by the extrapolated "best fit" and "maximum streamlining" lines in Figure 14.

Bearing the previously-stated assumption in mind that the A_r versus V_{water} relationship for target vegetation is described by Equation 18 for $V_w \leq 1.37$ m/s, we may draw some conclusions regarding the "book ending" of A_r values for $V_w > 1.37$ m/s. A_r values derived from the "maximum streamlining" assumption will be overestimates of A_r, as some streamlining, although perhaps minimal, can be expected to occur beyond 1.37 m/s. Consequently, this scenario can be expected to yield overestimates of drag forces and bending experienced by the tree. Conversely, A_r values derived from Equation 7 capture the "bottom end" of A_r and bending values as departure below the graph of this function is unlikely.

In sum, A_r values for $V_{water} \leq 1.37$ m/s will be computed using Equation 18. For $V_{water} > 1.37$ m/s, two A_r plots are considered (yielding two sets of corresponding bending predictions), one of which will be calculated using Equation 18, and the other will be constant with velocity and equal to 0.33, as per the "maximum streamlining" assumption.

This method for calculating A_r values in turn permits determination of streamlined frontal areas, A_f. This relationship is presented in Equation 19.

$$A_f = A_r A_0 \qquad (19)$$

In Equation 19, A_0 represents the nonstreamlined tree frontal area. Prior to bending tests, scaled digital photographs of nonstreamlined trees were taken. Nonstreamlined frontal areas, A_0, and tree heights, L, were then determined using Adobe Photoshop® and ImageJ software (Wayne Rasband, Research Services Branch, National Institute of Mental Health, Bethesda, Maryland).

The drag coefficient, C_d, can be calculated using nonstreamlined crown frontal areas, called "static C_d", or by using water-velocity-specific crown frontal areas, referred to as "dynamic C_d". As discussed above, this study utilizes the latter type of frontal areas. Accordingly, drag coefficients discussed henceforth are of the dynamic type.

Vollsinger et al. (2005) observed the dynamic C_d was relatively constant above wind speeds of 8 m/s (0.55 m/s water) for all species at a value of approximately 0.60. Accordingly, we use this value for the drag coefficient for computing drag forces for $V_{water} \geq 0.5$ m/s. However, a sensitivity analysis was performed to elucidate the effect of drag coefficient variability on predicted height ratios.

Having established a strategy for the calculation of A_f and C_d, the drag force experienced by a tree can be determined using Equation 15.

As stated earlier, previous studies investigating A_r relationships are scant, and to our knowledge none have examined relationships describing vegetation bending in terms of the reduced tree height, l (see Figure 15) as a function of velocity, which is a critical parameter (and the goal of this study) in estimating Manning's n and ultimately WSE for a given set of flow conditions.

In order to elucidate tree bending behavior due to flow-induced drag force, another significant simplifying assumption is made; the tree can be approximated as a tapered cylindrical cantilever beam of height L (determined using ImageJ software as described above) with a basal diameter, D_0, equal to that measured on the tree itself during the field tests. The diameter decreases linearly from the base to $D_0/10$ at height L.

The drag force, F_d, calculated in the manner described above resulting from the water velocity of interest is then conceptually applied to the beam uniformly. That is, the beam is subjected to a uniform line load, w, where

$$w = \frac{F_d}{l} \tag{20}$$

Therefore, the internal bending moment for a uniformly-loaded cantilever is given by (see Figure 15)

$$M = \frac{F_d}{2l}(2ly - y^2 - l^2) \tag{21}$$

Unlike the application of elastic beam theory for small deflections employed for the determination of E values, trees exposed to high flow will undergo large deflections. The governing elastic beam theory equation for large deflections becomes considerably more complicated as the beam now experiences both horizontal and vertical displacement. More specifically, the numerator of Equation 10 cannot be reduced to unity as was the case with small deflections as dx/dy can no longer be assumed to be near zero.

For brevity's sake, a less-detailed description of the tree bending prediction methodology follows (see Appendix IV for a detailed description). The bending of a cantilever beam experiencing large deflection is pictured in Figure 15 (note that the terms "tree" and "beam" are used interchangeably).

Ang Jr. et al. (1993) presented a numerical method applying a search procedure to solve the large deflection cantilever problem resulting from the application of a concentrated load at the beam's end. Chen (see Appendix IV) proposed a new approach based on the formulation by Ang Jr. et al. (1993) capable of predicting large deflections for tapered, cylindrical cantilevers subjected to uniform loads applied along the entire beam length.
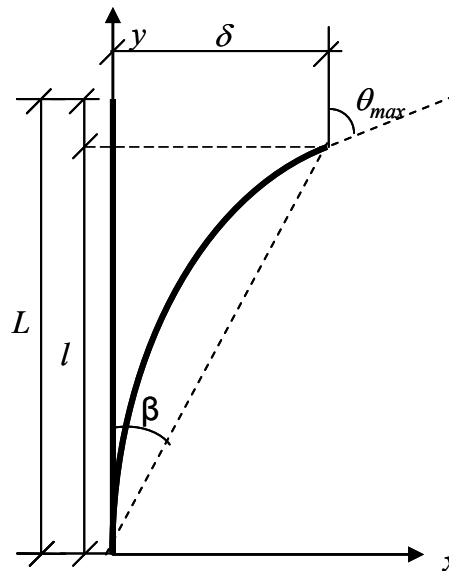
Figure 15. Large deflection of a cantilever beam. L represents the nonstreamlined beam height; l, streamlined beam height; σ, horizontal displacement; θmax, the maximum slope of the approximating beam; β the angle between the vertical axis originating at the beam base and a line connecting the beam base to the distal end.

Chen's method computes the length of the bent beam, i.e. the arc length, s(l), for a given l value (see Figure 15). If s(l) ≠ L, a new l value is assumed and the search procedure is repeated until the correct l is found such that s(l) = L. A numerical algorithm developed by Chen to perform the search procedure requires the drag force experienced by the tree, F_d, the tree's modulus of elasticity, E, the nonstreamlined tree height, L, and the diameter of the trunk at the base, D_0, as input parameters. The algorithm outputs vertical deflection, i.e., the reduced height of the tree due to bending, l, the beam's horizontal deflection, σ, the maximum slope of the approximating beam, $θ_{max}$, and the angle between the vertical axis originating at the beam base and a line connecting the beam base to the distal end, β (see Figure 15).

Figure 16 comprehensively describes the conceptual method employed in this study for the prediction of tree bending as a function of water velocity. The process can be broken down into four basic steps.
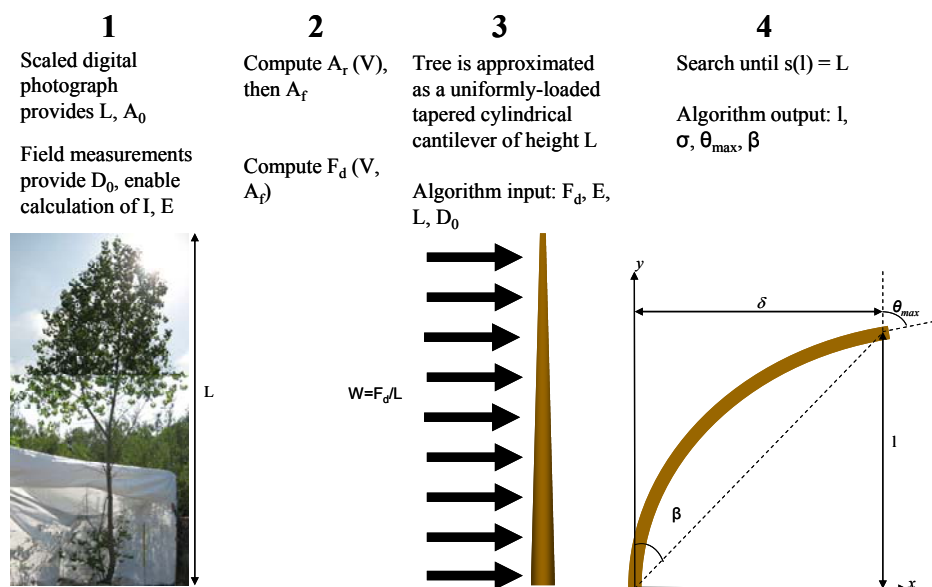
Figure 16. Comprehensive, conceptual tree bending prediction method.

CHAPTER 3

RESULTS

34 total tree pulling tests were conducted at the three field sites, including 6

cottonwoods, 12 willows, and 16 salt cedars. 8 salt cedar tests were deemed inadequate

for inclusion in this analysis, but will be included in a future work item addressing

vegetation washout, leaving 26 total trees for which bending was predicted. Data

collected from the tree pulling experiments was used to calculate values for the second

moment of area (I) and modulus of elasticity (E) for each tree (see Appendix I). Drag

forces acting on each tree for five water velocities (0.5, 1.0, 1.5, 2.0, and 2.5 m/s) were

then computed, followed by bending predictions for the same velocities. Two types of

bending predictions were performed for each tree, one guided by the "maximum

streamlining" A_r assumption, and the other by the "best fit" assumption described in the

methods section. Figure 17 contains bending predictions for one tree from each species

investigated in this study. Each graph represents a profile view of the tree as it undergoes

bending at different velocities with flow moving left to right. As expected, the trees

experienced a higher degree of bending with increased velocity.
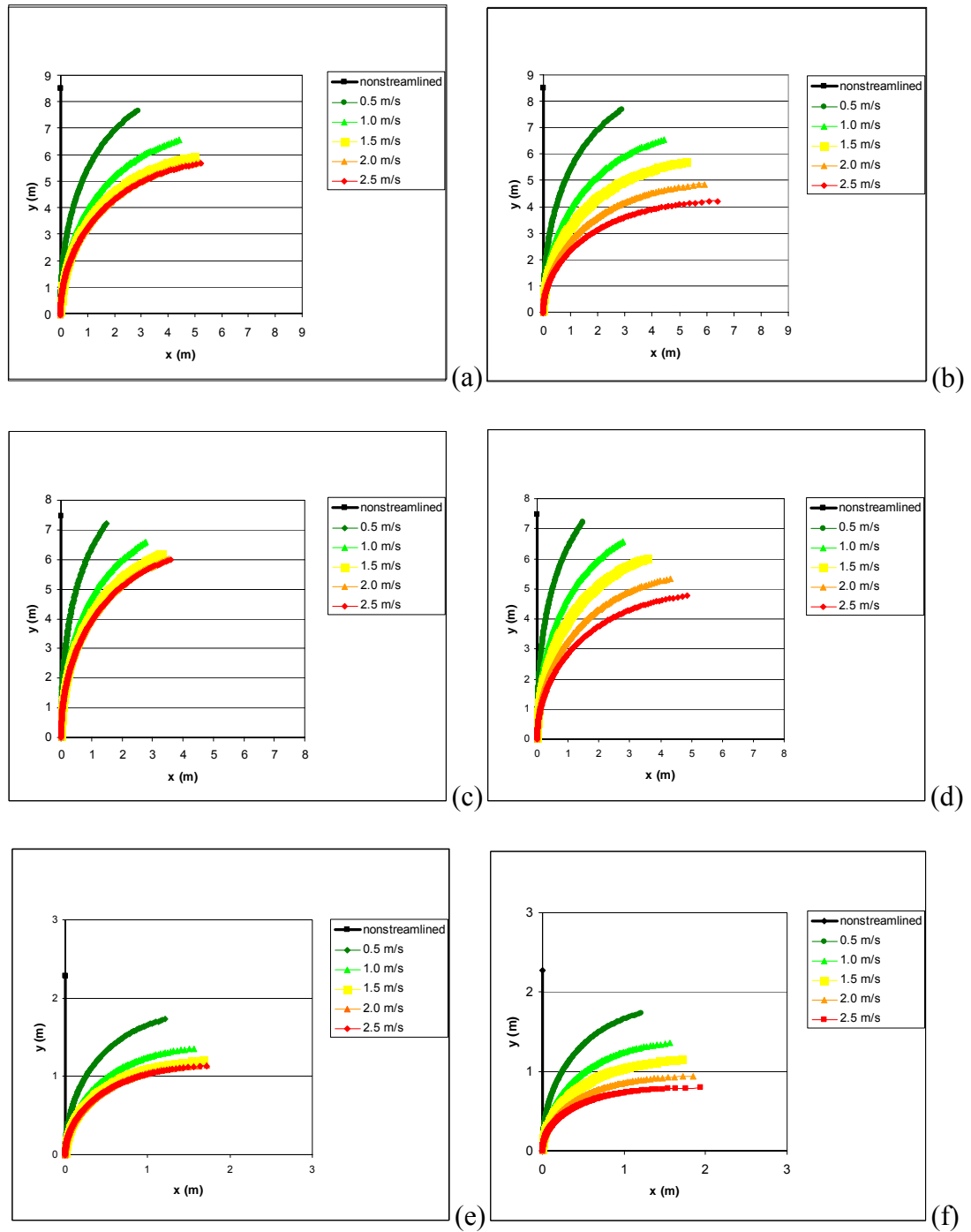
Figure 17. Bending predictions for a San Luis Rey River willow (a), a San Luis Rey River cottonwood (c), and a Las Vegas Wash salt cedar (e) resulting from the "best fit" frontal area ratio assumption. Bending predictions for the same trees, respectively, resulting from the "maximum streamlining" frontal area ratio assumption are depicted in graphs (b), (d) and (f).

Bending for water velocities equal to 0.5 and 1.0 m/s are the same for both A_r assumptions as the streamlined frontal areas for these velocities are guided by the "best fit" equation. As expected, bending predictions derived from the "maximum streamlining" assumption exhibit greater bending (lower H_r values) than those of the "best fit" assumption for water velocities of 1.5, 2.0, and 2.5 m/s as streamlined frontal area values for the "maximum streamlining" case will be larger than their "best fit" counterparts, and therefore result in larger drag forces and bending for a given velocity.

Figure 18 contains predicted height ratios (H_r) for all vegetation examined in the study for both the "best fit" and "maximum streamlining" assumptions. There is appreciable variability for the predicted H_r values; the range in variability increases with velocity. For example, at 2.5 m/s, H_r varies from 1.0 to 0.42 for the "best fit" assumption, and from 0.99 to 0.29 for the "maximum streamlining" case. The variability of predicted H_r values in Figure 18 is likely a manifestation of the extensive variance of plant characteristics and properties inherent in biological specimens.

In general, as expected, A_r values derived from the "maximum streamlining" assumption result in larger drag forces and predicted bending; this is manifested in the bulk of the H_r values being shifted downward in (b) for $V_{water} \geq 1.5$ m/s in comparison to (a) in Figure 18. Interestingly, no predicted H_r values are below 0.29. That is, no trees were expected to bend to a height lower than about 30% of their nonstreamlined height, even in water moving at 2.5 m/s (~ 8 ft/s).
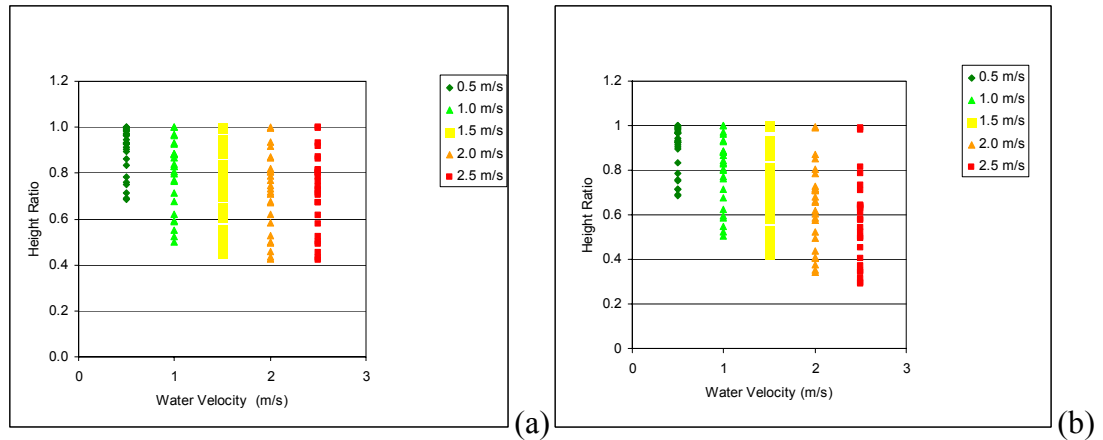
Figure 18. Predicted height ratios for all vegetation resulting from the (a) "best fit" and (b) "maximum streamlining" frontal area ratio assumptions.

Figure 19 below depicts predicted height ratios broken down by species. Each graph also contains a linear regression fit to the average of the predicted height ratios for each of the five water velocities examined. Two trees for each species lacked foliage. As expected, due to the appreciably lower drag forces experienced by such vegetation, predicted bending for these trees was significantly less than their counterparts with foliage. Consequently, trees lacking foliage are omitted from these figures as their bending behavior differs appreciably. The data in Figure 19 is summarized in Table 1 below. Figure 20 and Table 2 contain height ratio data broken down by species for those trees lacking foliage.
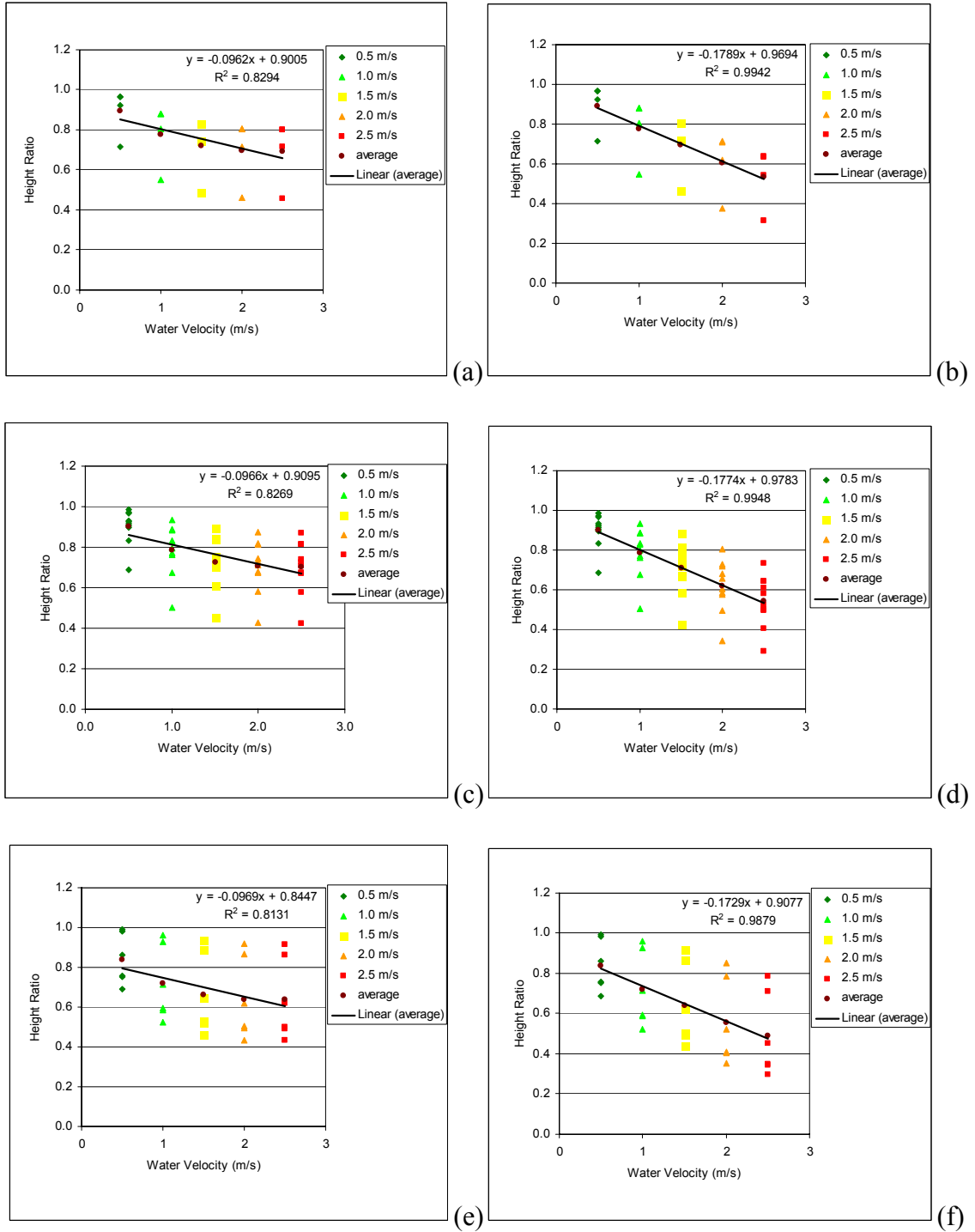
Figure 19. Predicted height ratios for cottonwoods (a), willows (c), and salt cedars (e) resulting from the "best fit" frontal area ratio assumption. Predicted height ratios for the same trees, respectively, resulting from the "maximum streamlining" frontal area ratio assumption are depicted in graphs (b), (d) and (f). Vegetation lacking foliage is omitted from the graphs.

Table 1. Average, minimum, and maximum predicted height ratios resulting from both the "best fit" and "maximum streamlining" frontal area ratio assumptions. Vegetation lacking foliage is omitted from the table.

Species	Ar method	V	Avg. Hr	Min. Hr	Max. Hr
cottonwoods	"best fit"	0.5	0.89	0.72	0.97
		1.0	0.78	0.55	0.88
		1.5	0.72	0.48	0.83
		2.0	0.70	0.46	0.81
		2.5	0.69	0.46	0.80
	"max. streamlining"	0.5	0.89	0.72	0.97
		1.0	0.78	0.55	0.88
		1.5	0.70	0.46	0.81
		2.0	0.60	0.37	0.71
		2.5	0.53	0.31	0.64
willows	"best fit"	0.5	0.90	0.69	0.99
		1.0	0.79	0.50	0.93
		1.5	0.73	0.45	0.89
		2.0	0.71	0.43	0.87
		2.5	0.69	0.42	0.87
	"max. streamlining"	0.5	0.90	0.69	0.99
		1.0	0.79	0.50	0.93
		1.5	0.71	0.42	0.88
		2.0	0.62	0.34	0.81
		2.5	0.54	0.29	0.73
salt cedars	"best fit"	0.5	0.84	0.69	0.99
		1.0	0.72	0.52	0.96
		1.5	0.66	0.46	0.93
		2.0	0.64	0.44	0.92
		2.5	0.64	0.43	0.92
	"max. streamlining"	0.5	0.84	0.69	0.99
		1.0	0.72	0.52	0.96
		1.5	0.64	0.44	0.92
		2.0	0.55	0.35	0.85
		2.5	0.49	0.30	0.79
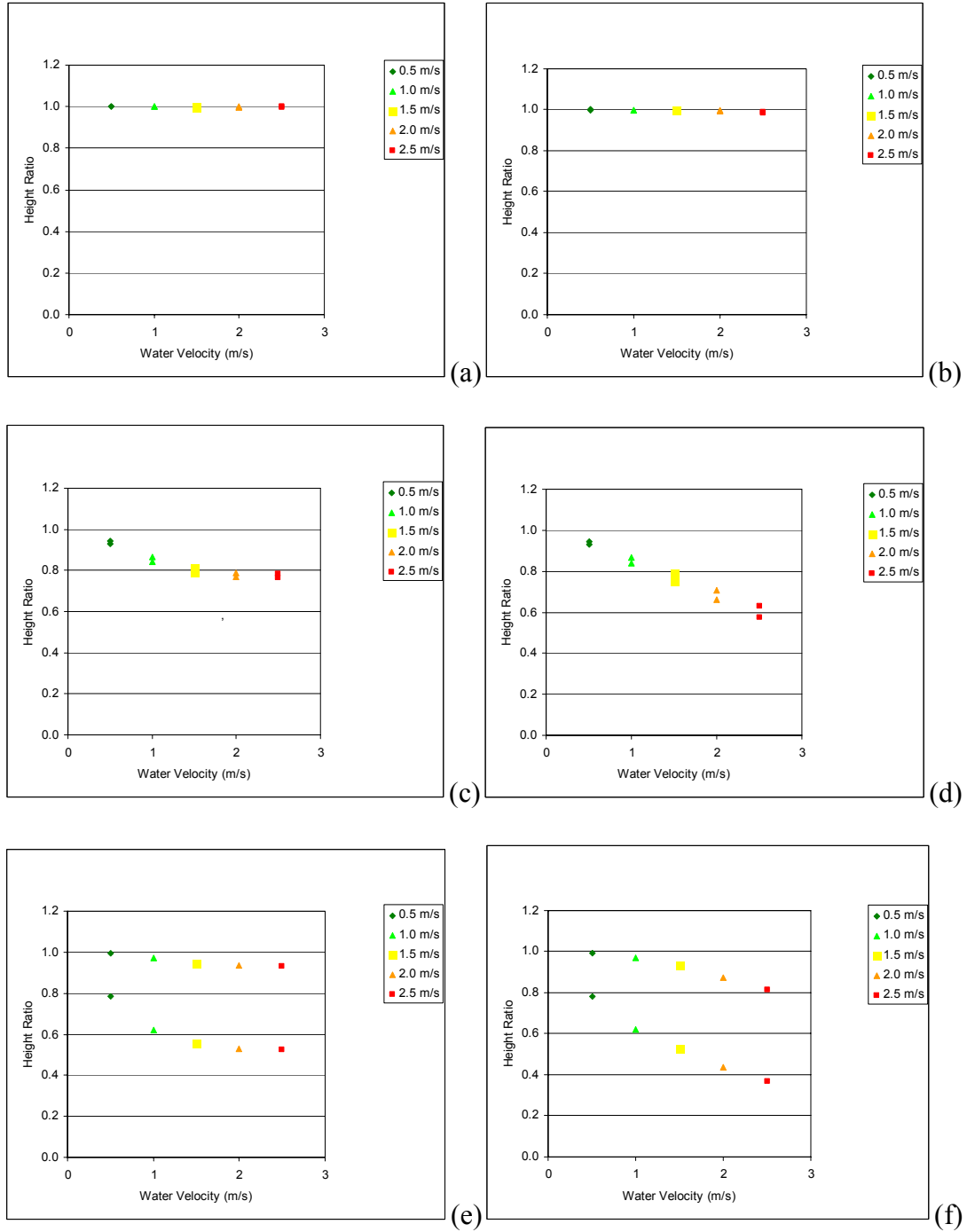
Figure 20. Predicted height ratios for cottonwoods (a), willows (c), and salt cedars (e) resulting from the "best fit" frontal area ratio assumption. Predicted height ratios for the same trees, respectively, resulting from the "maximum streamlining" frontal area ratio assumption are depicted in graphs (b), (d) and (f). Only vegetation lacking foliage is included in the graphs.

Table 2. Average, minimum, and maximum predicted height ratios resulting from both the "best fit" and "maximum streamlining" frontal area ratio assumptions. Only vegetation lacking foliage is included in the table.

Species	Ar method	V	Avg. Hr	Min. Hr	Max. Hr
cottonwoods	"best fit"	0.5	1.00	1.00	1.00
		1.0	1.00	1.00	1.00
		1.5	1.00	1.00	1.00
		2.0	1.00	1.00	1.00
		2.5	1.00	1.00	1.00
	"max. streamlining"	0.5	1.00	1.00	1.00
		1.0	1.00	1.00	1.00
		1.5	1.00	1.00	1.00
		2.0	1.00	1.00	1.00
		2.5	0.99	0.99	0.99
willows	"best fit"	0.5	0.94	0.93	0.94
		1.0	0.85	0.84	0.87
		1.5	0.80	0.79	0.81
		2.0	0.78	0.77	0.79
		2.5	0.77	0.76	0.78
	"max. streamlining"	0.5	0.94	0.93	0.94
		1.0	0.85	0.84	0.87
		1.5	0.77	0.75	0.79
		2.0	0.69	0.66	0.71
		2.5	0.60	0.58	0.63
salt cedars	"best fit"	0.5	0.89	0.78	0.99
		1.0	0.80	0.62	0.97
		1.5	0.75	0.55	0.95
		2.0	0.73	0.53	0.93
		2.5	0.73	0.52	0.93
	"max. streamlining"	0.5	0.89	0.78	0.99
		1.0	0.80	0.62	0.97
		1.5	0.73	0.53	0.93
		2.0	0.65	0.44	0.87
		2.5	0.59	0.37	0.81

Statistical Analyses

In order to examine the effects of velocity on H_r between species, a 5 (velocity) x 3 (species) factorial ANOVA was conducted. H_r values for this and the analyses to follow

were derived from A_r values as per the "best fit" assumption only unless noted otherwise. The main effects of velocity on H_r was significant, $F(4,85)=15.097$, $p<.001$. $R^2=.439$, $p<.001$.

Although bending behavior between species was observed to be different, the ANOVA revealed there was no statistically significant difference in H_r between species, $F(2,85)=1.747$, $p=.181$, non. sig. Figure 21 reveals that cottonwood and willow bending behavior was quite similar whereas salt cedar appeared to bend more readily for a given velocity. Thus, a follow-up analysis was conducted.
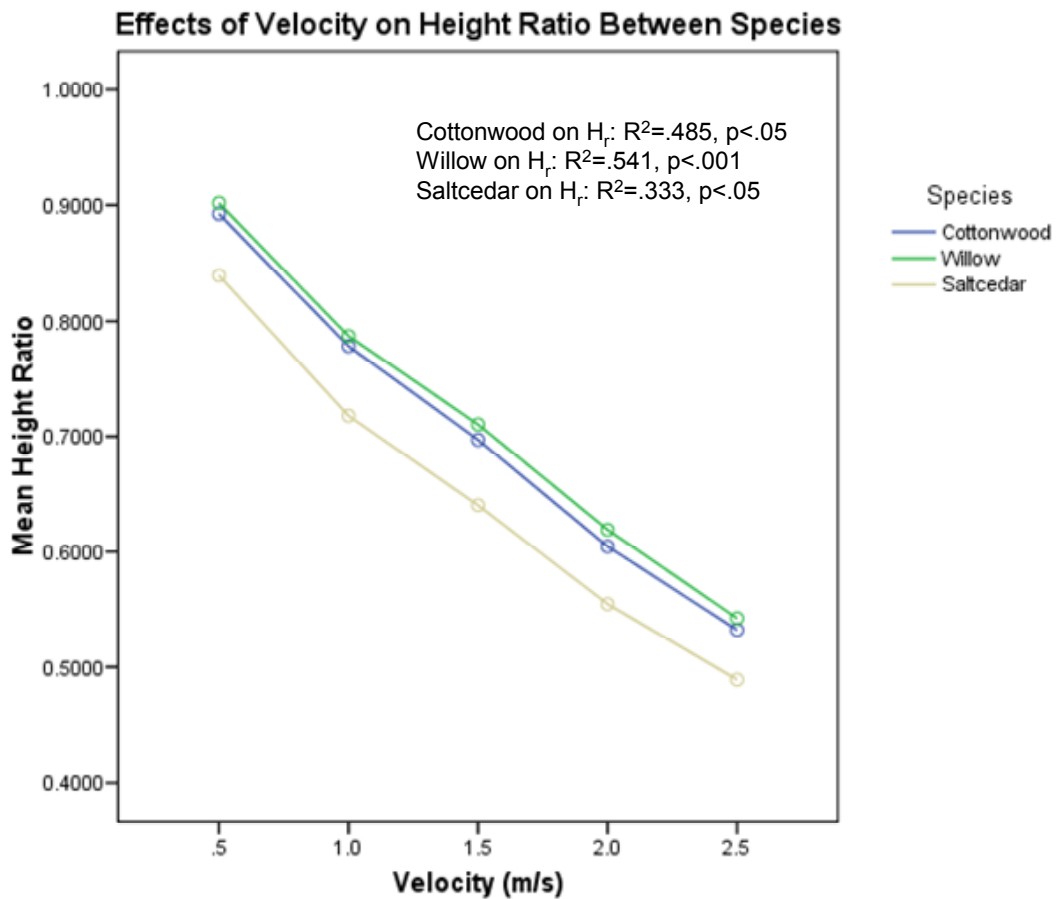
Figure 21. Effect of species on height ratio.

Because of the anecdotal evidence and of the significant difference in elasticity between salt cedar and the other two species, the height ratio data for cottonwoods and willows was collapsed into one data set to examine whether the mean height ratio of salt cedar was significantly different from that of cottonwood and willow. An independent t-test was conducted, and the results showed that the main effect of velocity was marginally significant on height ratio, $t(1,90)=3.612$, $p=.061$. Its statistically non-significant results could be explained by lack of statistical power due to the small sample size.

Elasticity values were observed to vary substantially both within and between species. A one-way ANOVA was conducted to examine whether elasticity changed as a function of species. The results showed a significant difference in the mean elasticity between species, $F(2,23)=4.865$, $p<.05$. Post-hoc analyses revealed that the mean elasticity of salt cedar was significantly lower than that of cottonwood, $t(2,12)=2.184$, $p<.05$, and that of willow, $t(2,15)=3.446$, $p<.005$. There was no statistical significance in elasticity between cottonwood and willow, $t(2,16)=1.237$, $p=0.234$, non. sig. This observation supports the results of the bending experiments in that cottonwoods and willows displayed similar characteristics that were different from salt cedar. Elasticity did not correlate with any other plant dimensions in this study, which is to be expected as elasticity is a material property independent of plant dimensions.

A source of uncertainty within the drag force equation, and therefore in the bending predictions themselves, is tree frontal area. To elucidate this uncertainty, a one-way ANOVA was conducted on A_r and H_r to examine whether the selection of high, low, or mean A_r values from the range of data published by Vollsinger et al. (2005) would result

in statistically significantly different A_r and H_r values. Height ratio predictions were

performed for water velocities of 0.27, 0.55, 0.82, 1.10, and 1.37 m/s using the minimum

(MIN) and maximum (MAX) observed frontal area ratios for the five species examined

by Vollsinger et al. (2005) (see Figure 22) and those predicted by the "best fit" (BEST)

frontal area assumption for each velocity, for a typical willow, cottonwood, and salt

cedar. The results showed the main effect of A_r methods on A_r, $F_{(2,42)}=4.952$, $p<.05$.

Post-hoc analyses revealed that A_r for MIN was not statistically different than that for

BEST, $t_{(1,28)}=1.317$, $p=.198$, non. sig. A_r for MIN was statistically less than that for

MAX, $t_{(1,28)}=3.024$, $p<.05$. The statistical difference between A_r for BEST and MAX

were marginally significant, $t_{(1,28)}=1.892$, $p=.069$. There was no statistical significance

on H_r, $F_{(2,42)}=1.748$, $p=.187$. In other words, H_r is insensitive to selection of A_r methods

even though the resultant A_r values were significantly different for these "low" water

velocities.
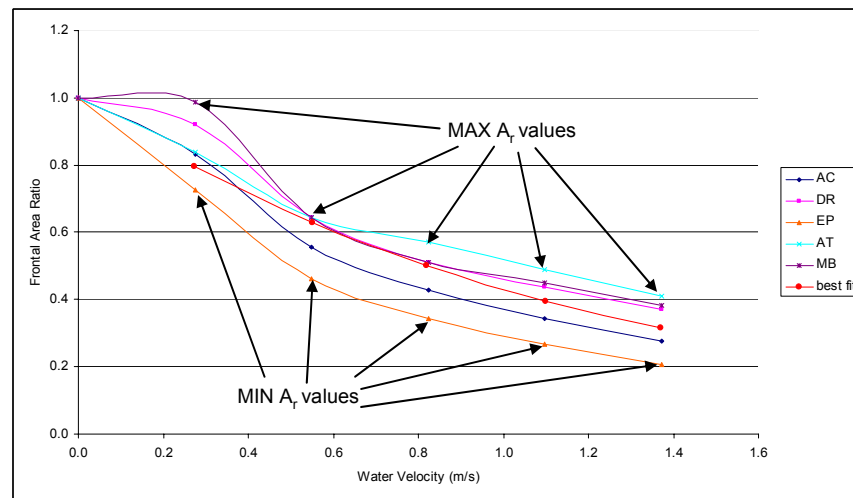
Figure 22. Frontal area ratio of unpruned crowns of black cottonwood (AC), red alder (DR), paper birch (EP), trembling aspen (AT) and bigleaf maple (MB) as a function of water velocity. MIN and MAX frontal area ratio values used to determine the effect of Ar choice on Hr for low velocities are highlighted (modified from Vollsinger et al., 2005).

In order to examine the sensitivity of H_r value to A_r methods at high velocities (1.5 2.0, and 2.5 m/s), an independent sample t-test on H_r was conducted. The A_r methods examined for this analysis included the "best fit" and "maximum streamlining" (MAXSTR) assumptions (see Figure 14). The results showed that there was a significant difference in H_r values between A_r methods, $t(1, 118)=2.884$, $p<005$, such that H_r for BEST was significantly higher than that for MAXSTR. A series of independent sample t-tests were then conducted to investigate whether different A_r methods resulted in significantly different H_r values. The results showed that there was no statistical difference between H_r values between different A_r methods at V=1.5 m/s, $t(1, 38)=0.410$, $p=.68$, non. sig. At V=2.0 m/s, there was a marginally significant difference between groups, $t(1, 38)=1.759$, $p=.087$, such that H_r for BEST was higher than that of MAXSTR. At V=2.5 m/s, the difference between groups became significant, $t(1, 38)=2.942$, $p<.01$ with the same trend. In other words, the higher the velocity was the more H_r became sensitive to different A_r methods. This suggests for higher velocities, frontal area ratio choice has a potentially significant effect on predicted height ratio, and therefore on channel roughness and water surface elevation as well. Therefore, for higher velocities, care must be exercised in frontal area ratio selection as there are potentially grave consequences in its misapplication. To our knowledge, there are no studies investigating the frontal area streamlining behavior of woody riparian species for this range of water velocities, so the need for research in this area is apparent.

An additional source of uncertainty within the drag force equation exists in the drag coefficient. In order to investigate the effects of C_d method on H_r, a one-way ANOVA was conducted on H_r. The results showed that there was no statistical significance on H_r

between different C_d method, $F(2,42)=0.729$, $p=.489$, non. sig. Therefore, reasonable but differing choices for the drag coefficient are unlikely to elicit substantially different tree bending predictions.

CHAPTER 4

DISCUSSION

Predicted height ratios display considerable variability for all velocities examined, ranging from no detectable bending ($H_r = 1.0$) to a minimum height ratio of 0.29. The variability of predicted H_r values both within and between species is likely a manifestation of the extensive variance of tree elasticity and second moment of area values inherent in biological specimens. However, the linear regressions fitted to the mean H_r for each velocity (see Figure 19) suggest statistically significant correlations. Although significant differences existed in measured elasticity values, predicted height ratios did not differ significantly between species. Only when predicted height ratios for cottonwoods and willows were collapsed did salt cedars appear marginally significantly different. However, these differences might be masked due to the limited sample size of the study.

A tree's true A_r relationship will deviate from that described by the "best fit" equation. For instance, a tree with an appreciably higher elasticity value than those examined previously from which the "best fit" equation (Equation 18) derives would likely streamline less than the "best fit" tree, hence its A_r values will be higher, while its H_r values will be lower in comparison, and vice versa. Similarly, a tree with appreciably larger diameter trunks and limbs will behave in the same manner compared to the tree described by the "best fit" A_r function. Indeed, the trees examined in this study could be more accurately described by an A_r function differing from the "best fit" one. However, as discussed in the statistical analyses above, such differences are unlikely to have a significant effect on prediction of H_r as H_r was insensitive to selection of A_r for low ($\leq$

44

1.37 m/s) water velocities. More specifically, tested area ratio values differing by as much as 30% from the "best fit" value for a particular velocity were found to produce less than a 5% difference in predicted H_r. Therefore, for trees with foliage at low (≤ 1.37 m/s) water velocities, the "best fit" equation provides a sound estimate for frontal area ratio.

The assumption made regarding the dynamic drag coefficient ($C_d = 0.6$ for $V_{water} \geq 0.5$ m/s) is valid as well, as no statistical significance on H_r between C_d choice was found. More specifically, drag coefficients equal to 0.5 and 0.7 were examined in this particular sensitivity analysis, both of which encapsulate the variation observed by Vollsinger et al. (2005) for all five hardwood species examined in that study. Moreover, dynamic drag coefficient values in the Vollsinger et al. (2005) study asymptote to 0.6 with increasing velocity so the assumption made in this study is valid for both low (≤ 1.37 m/s) and high (> 1.37 m/s) velocities.

For the "high" velocities (1.5, 2.0, and 2.5 m/s) examined in this study, H_r was insensitive to A_r choice for 1.5 and 2.0 m/s. Therefore, both the "best fit" and "maximum streamlining" assumptions provide reasonable methods for estimation of A_r for these velocities, and either may be employed without detriment to H_r prediction. However, the engineer tasked with making a conservative estimate (or "worse case" scenario) regarding increased water surface elevation due to vegetation encroachment would be advised to select the "best fit" A_r approximation method, as doing so produces a lower A_r, hence lower drag force, higher resultant H_r, and greater hydraulic roughness and water surface elevation than that provided by the "maximum streamlining" method.

Statistical analyses revealed H_r was sensitive to A_r choice at a water velocity of 2.5 m/s. Therefore, caution should be exercised in interpreting H_r predictions presented in this study for this velocity (see Figure 16). Furthermore, in light of this fact, the importance of elucidating A_r relationships in future studies for a variety of vegetation for high velocities becomes increasingly apparent.

Figure 19 contains linear regression equations fitted to the mean height ratio versus velocity plots for each of the three species examined in this study resulting from the "maximum streamlining" and "best fit" frontal area ratio assumptions. Data for trees lacking foliage are omitted from the regression calculations. In light of the acceptability of this study's simplifying A_r and C_d assumptions in the preceding paragraphs, these regression equations provide a reasonable method for H_r estimation for low velocities, and therefore offer an alternate, although less individualized, method for H_r estimation to the "comprehensive" method described herein (see Figure 16). However, due to the considerable variability of predicted H_r values for a given velocity (see Figure 19 and Table 1), which is attributed to the extensive variance of plant characteristics and properties inherent in biological specimens, caution should be exercised in interpretation of these values, particularly for water velocities near 2.5 m/s. That is to say, by opting for this less individualized, less work intensive approach, accuracy of H_r prediction is sacrificed as individual plant characteristics including elasticity and second moment of area are not accounted for. Alternatively, a probability-based approach could be attempted in the future by collecting substantially more data.

Again, as was the case regarding selection of A_r prediction method, the engineer tasked with making a conservative estimate regarding increased water surface elevation

due to vegetation encroachment would be advised to select the regression equation fitting H_r values derived from the "best fit" A_r approximation method, as doing so would result in higher water surface elevations than that provided by the "maximum streamlining" method. Furthermore, an even more conservative estimate would be guided by the maximum predicted H_r values for each species, identified by blue arrows in Figure 23 below.

Recommendations concerning height ratios for trees lacking foliage are difficult to make due to small sample size. As expected, trees lacking foliage will experience lower drag forces than they would if foliage were present, and therefore bend less. This phenomenon was described in Figure 20 and Table 2 above.

Interestingly, these results suggest none of the vegetation examined in this study will bend to the degree that it lays flat on the channel bed. In fact, the smallest predicted height ratio was approximately 0.3. That is, no trees were expected to bend so greatly that they were reduced to lower than about 30 percent of their original, nonstreamlined height. This suggests that a channel exhibiting encroachment by vegetation similar to that examined in this study (which appears to be commonplace throughout the Southwestern United States) will experience significant roughness and conveyance impedance during high flow events. Consequently, water surface elevations during such an event have the potential to exceed channel design capacity, therefore increasing the risk for destruction of habitat, property, and loss of life.
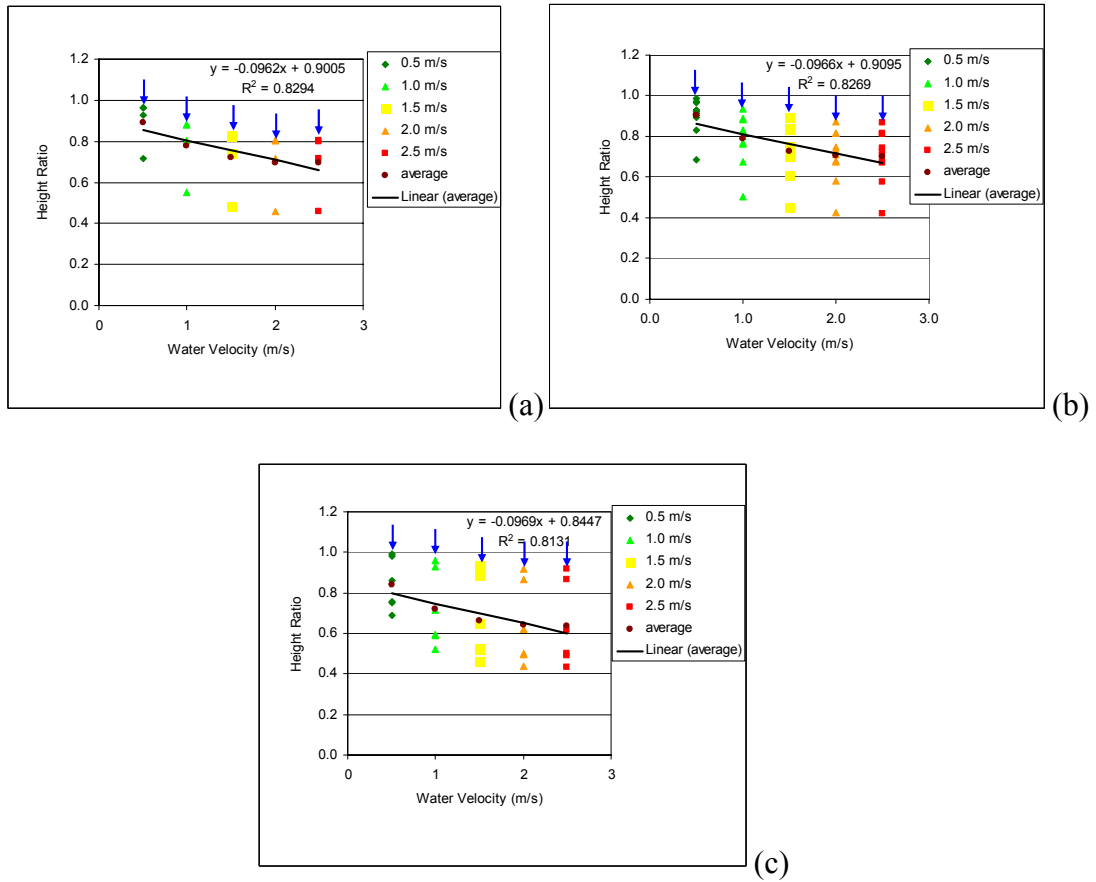
Figure 23. Predicted height ratios resulting from the "best fit" frontal area ratio assumption for (a) cottonwoods, (b) willows, and (c) salt cedars. Maximum predicted height ratios for each velocity are indicated by blue arrows and provide a conservative estimate for streamlined vegetation height for the calculation of channel roughness and ultimately water surface elevation.

CHAPTER 5

STUDY LIMITATIONS AND

RECOMMENDATIONS

In regard to the field test methodology employed for the determination of E values in this study, it is recommended the specimen be pulled in an incremental, stepwise fashion rather than in one continuous motion. Doing so permits the collection of numerous applied force versus bending angle paired values for each step, thereby enhancing the robustness of the data set.

In contrast to temperate forest trees, woody riparian species often exhibit multiple main trunks and stems near the base of the plant. For these trees, the winching sling was wrapped around the entire tree and lashed in place with rope to prevent slippage during the pull (see Figure 24).

Before initiation of the pull test, the sling was cinched down manually as tightly as possible, which resulted in the basal stems being drawn toward the center into close proximity to one another. Unfortunately it was not always possible to completely cinch multiple stems together prior to each test. This becomes problematic when attempting to compute E values from the field test data. Ideally, as is the case with single trunk trees and multiple stemmed trees for which complete pre-test cinching was achieved, all force applied by the winch on the tree contributes entirely to bending of the tree. However, in the case of multiple-stemmed trees in which complete pre-test sling cinching was not possible, upon initiation of the pull test some of the force applied by the winch contributes to cinching of the sling and not entirely to tree bending. That is, the strain gage will register increasing force with time as the sling cinches the stems together, but

that force has not contributed to tree bending. Therefore, applied force versus bending

angle data is deceptive for these cases, resulting in questionable E values.

Figure 24. Tree pulling sling attachment to salt cedar tree.

Although occasionally problematic with regard to E computation, this sling

configuration was not employed arbitrarily, as the objective of our pulling tests were not

solely to elucidate tree bending properties. An attempt was made to pull test trees

completely from the ground in order determine their failure properties (for a future work

item), which required the robust configuration offered by the attachment method

employed here.

For future work in which only elasticity values are sought, it would be advantageous

to attach the pull line to single primary trunks or stems and conducting multiple pulling

tests as needed, thereby circumnavigating cinching hindrances.

In addition, weighing the entire specimen upon conclusion of each pull test if possible

is recommended, as previous work conclusively demonstrates the predictive relationship

between tree mass and both drag force and critical failure moment.

Additional flume studies investigating the relationships between H_r, A_r, C_d, F_d and velocity for woody riparian species varying in size, age, and crown morphology for velocities simulating those anticipated during high flow events for both submerged and emergent cases would prove an indispensible resource in mitigating flood risks due to vegetation encroachment.

While the assumptions adopted in this study have provided a simplified but useful starting point from which to work for the prediction of vegetation bending, it is suggested that those assumptions be adapted further in a manner that more closely approximates the "real" conditions likely to be encountered in high streamflow events. Namely, the predictive algorithm should be capable of accommodating non-uniformly loaded cantilevers as this will permit more accurate calculation of drag forces experienced by the tree arising from non-uniform water velocity profiles and frontal area heterogeneity. Additionally, scaling issues warrant further research. Namely, the effect of vegetation community composition on individual bending should be investigated. Scouring of channel bed material also likely influences bending and most certainly vegetation failure and washout; tree pulling tests elucidating the effect of bed scour on bending and failure are recommended.

This study provides a method for calculating the bending of woody riparian vegetation as a function of water velocity, which in turn can be used to estimate hydraulic roughness. However, when considering the question of water surface elevations for large flow events in channels exhibiting vegetation encroachment, velocity will be unknown, and it is the streamflow which is known. To complicate matters further, as has been demonstrated in this study, vegetation bending, and hence Manning's n, is a function of

velocity, and vice versa. A future work item will provide a method for determining hydraulic roughness, n, and water surface elevation that considers the bending of vegetation.

CHAPTER 6

CONCLUSION

Vegetation encroachment reduces channel conveyance capacity below design objectives and greatly increases the risk for loss of life and property damage in the case of large flood events. Given minimal knowledge of hydraulic roughness for shrubs and woody vegetation, accurate estimation of channel capacity and water surface elevation is difficult, particularly because hydraulic roughness is not only a function of individual plant characteristics and community composition, but varies with water depth and velocity as plants deform with flow. Fischenich (2000) proposed Equation 2 for the prediction of Manning's n for emergent and submerged vegetation based on the concepts of drag. The ability to predict how a plant bends, or more specifically, how its height changes in the presence of flow, is required for effective usage of Fischenich's (2000) equation. In sum, elucidation of plant height ratios as a function of water velocity permits more accurate prediction of hydraulic roughness and water surface elevation.

The purpose of this study was to quantify the height ratios of woody riparian species as a function of water velocity. This was accomplished through a series of field tests to elucidate tree bending properties which in turn serve as input parameters for a numerical algorithm designed to predict tree bending for water velocities likely to be encountered during high flow events. This study focused on key riparian species of the Southwestern United States; however, techniques are generic in nature and analogous data may be collected for additional riparian and terrestrial species.

34 total tree pulling tests were conducted at three field sites, including 6 cottonwoods, 12 willows, and 16 salt cedars. 8 salt cedar tests were deemed inadequate for inclusion in

this analysis, but will be included in a future work item addressing vegetation washout. Upon calculation of E and F_d values for the 26 remaining tests, bending predictions were conducted for five water velocities (0.5, 1.0, 1.5, 2.0, and 2.5 m/s). Two bending predictions based on differing methods for estimating streamlined tree frontal areas were performed for each tree.

Predicted height ratios display considerable variability for all velocities examined, ranging from no detectable bending ($H_r = 1.0$) to a minimum height ratio of 0.29. The variability of predicted H_r values is likely a manifestation of the extensive variance of tree elasticity and second moment of area values inherent in biological specimens.

No trees were expected to bend so greatly that they were reduced to lower than about 30 percent of their original, nonstreamlined height. This suggests that a channel exhibiting encroachment by vegetation similar to that examined in this study (which appears to be commonplace throughout the Southwestern United States) will experience significant roughness and conveyance impedance during high flow events. Consequently, water surface elevations during such an event have the potential to exceed channel design parameters, therefore increasing the risk for destruction of habitat, property, and loss of life.

Future work should seek to elucidate bending for a variety of riparian species for high water velocities in laboratory studies. A method for determining hydraulic roughness, n, and water surface elevation that considers the bending of vegetation is warranted. Such a method should address scaling issues, as community composition promises to play a salient role in influencing water surface elevation. In addition, the role of bed scour on vegetation bending and failure is recommended.

APPENDIX I

FIELD EXPERIMENT RESULTS

Species	Tree ID	L (m)	A_0 (m^2)	I (m^4)	E (MPa)
cottonwood	rg cw2	6.21	2.08	6.74E-05	1963
	rg cw1	5.06	0.82	2.87E-05	1999
	slr cw1	5.44	10.11	2.10E-05	522
	slr cw3	7.48	8.18	1.02E-05	2536
	slr cw2	7.90	7.78	6.31E-06	4228
	slr cw4	2.12	1.12	7.37E-08	1528
	avg	5.70	5.01	2.23E-05	2129
	stdev	2.08	4.12	2.44E-05	1230
willow	slr wi10	9.54	13.45	5.15E-05	2790
	slr wi8	10.60	7.33	2.87E-05	1667
	slr wi4	7.13	7.16	2.62E-05	531
	slr wi9	8.51	8.83	6.31E-06	2501
	slr wi3	4.80	3.03	1.45E-06	1308
	slr wi1	5.14	3.05	8.96E-07	2326
	rg wi1	2.54	0.51	1.16E-07	2776
	slr wi7	4.11	0.40	5.82E-08	5678
	rg wi2	2.26	0.27	5.65E-08	1813
	slr wi2	3.97	0.37	3.98E-08	5354
	slr wi6	4.44	0.69	3.02E-08	7616
	slr wi5	3.78	0.80	1.92E-08	5518
	avg	5.57	3.83	9.62E-06	3323
	stdev	2.73	4.35	1.68E-05	2175
salt cedar	lvw sc9	5.08	18.88	4.49E-04	113
	lvw sc2	3.45	5.26	9.60E-06	1059
	lvw sc1	4.71	5.83	6.71E-06	246
	rg sc1	3.61	0.78	2.32E-06	1560
	slr sc1	2.99	3.56	1.25E-06	645
	rg sc2	3.55	0.49	3.32E-07	441
	lvw sc4	2.61	1.76	1.03E-07	1275
	lvw sc13	2.28	1.17	5.13E-08	2390
	avg	3.53	4.72	5.87E-05	966
	stdev	0.96	6.07	1.58E-04	766

APPENDIX II

TREE BENDING PREDICTION GRAPHS

Figure II.1. Bending prediction for Rio Grande Cottonwood 1 resulting from "best fit" (a) and "maximum streamlining" (b) frontal area ratio assumptions.

Figure II.2. Bending prediction for Rio Grande Cottonwood 2 resulting from "best fit" (a) and "maximum streamlining" (b) frontal area ratio assumptions.
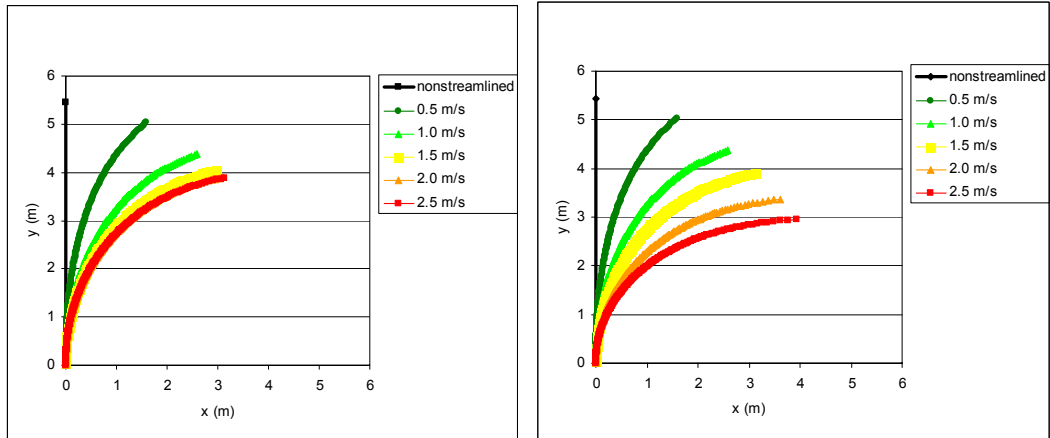
Figure II.3. Bending prediction for San Luis Rey Cottonwood 1 resulting from "best fit" (a) and "maximum streamlining" (b) frontal area ratio assumptions.
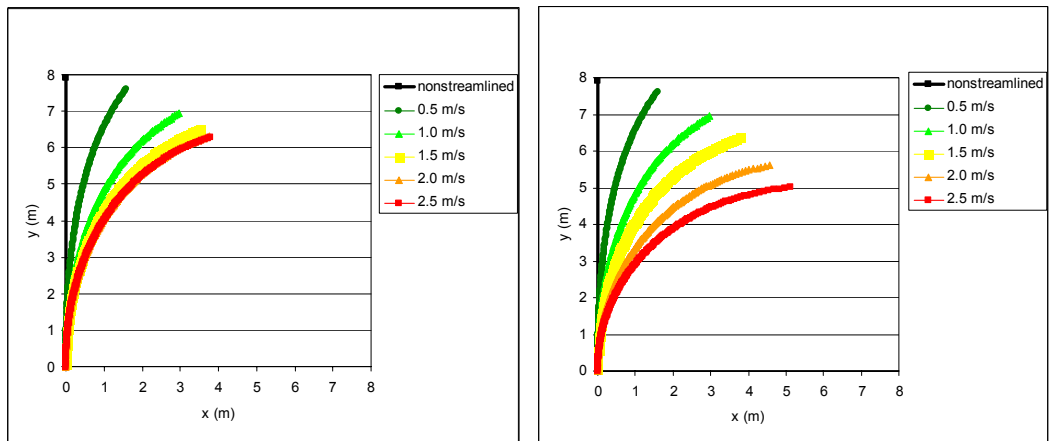
Figure II.4. Bending prediction for San Luis Rey Cottonwood 2 resulting from "best fit" (a) and "maximum streamlining" (b) frontal area ratio assumptions.
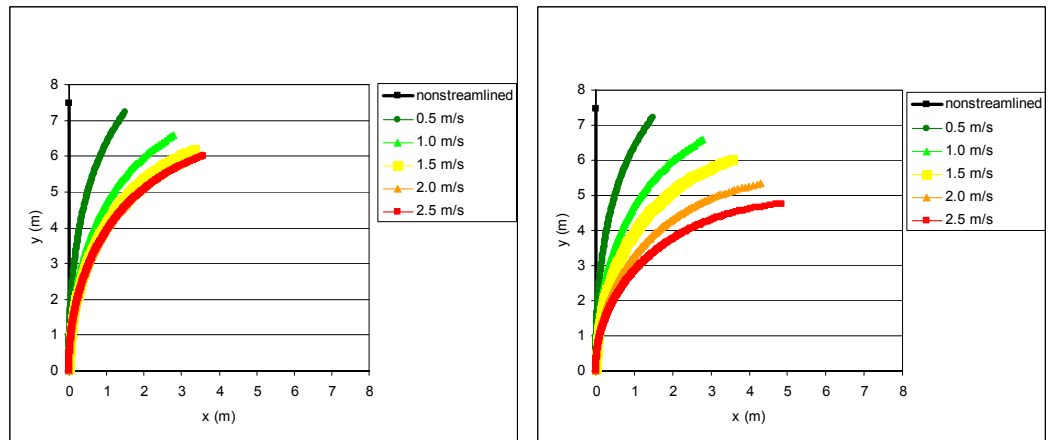
Figure II.5. Bending prediction for San Luis Rey Cottonwood 3 resulting from "best fit" (a) and "maximum streamlining" (b) frontal area ratio assumptions.
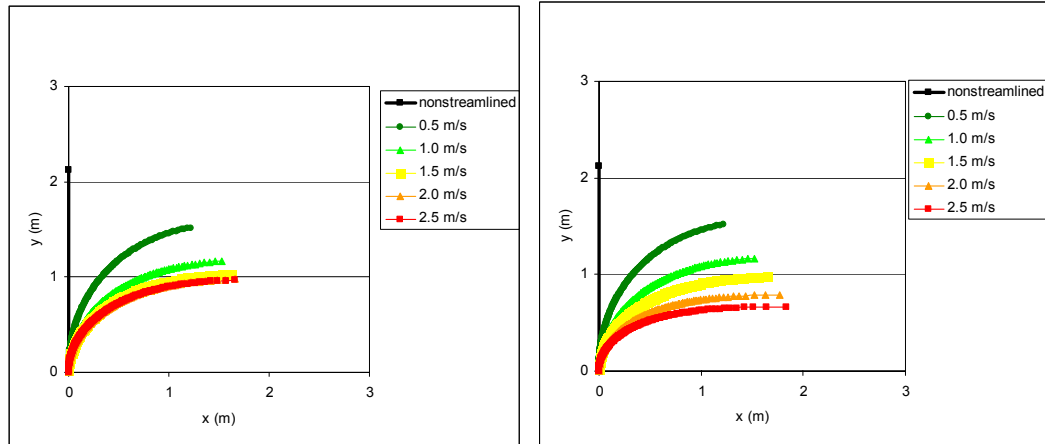
Figure II.6. Bending prediction for San Luis Rey Cottonwood 4 resulting from "best fit" (a) and "maximum streamlining" (b) frontal area ratio assumptions.
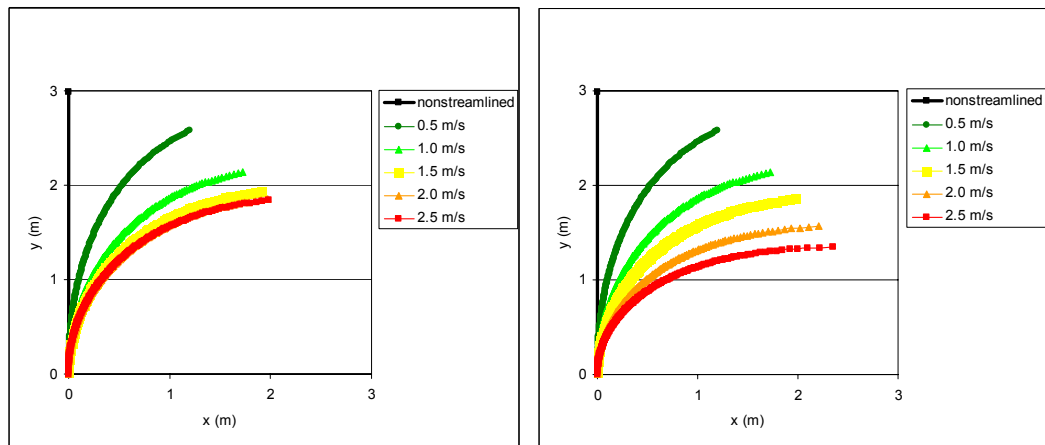
Figure II.7. Bending prediction for San Luis Rey Salt Cedar 1 resulting from "best fit" (a) and "maximum streamlining" (b) frontal area ratio assumptions.
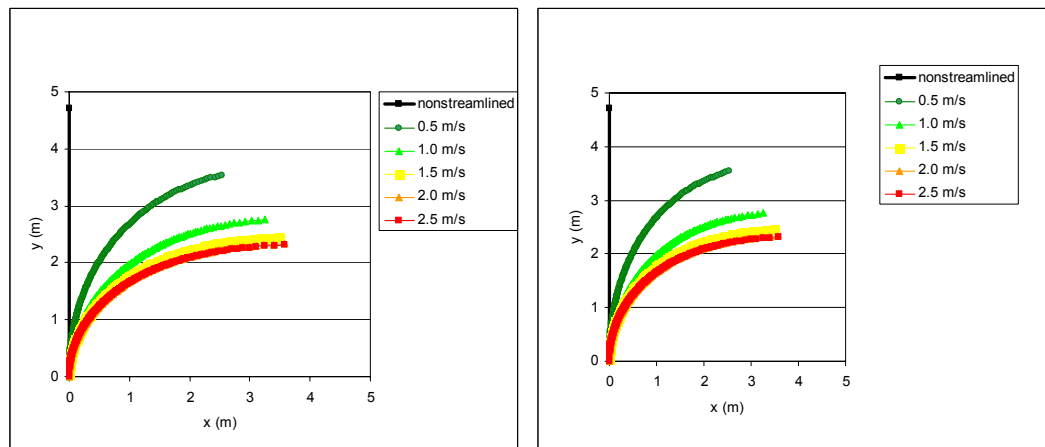
Figure II.8. Bending prediction for Las Vegas Wash Salt Cedar 1 resulting from "best fit" (a) and "maximum streamlining" (b) frontal area ratio assumptions.
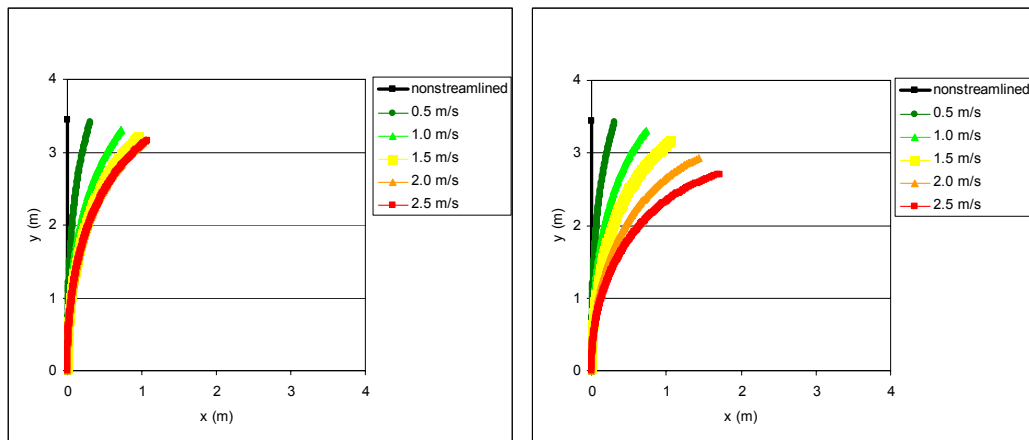
Figure II.9. Bending prediction for Las Vegas Wash Salt Cedar 2 resulting from "best fit" (a) and "maximum streamlining" (b) frontal area ratio assumptions.
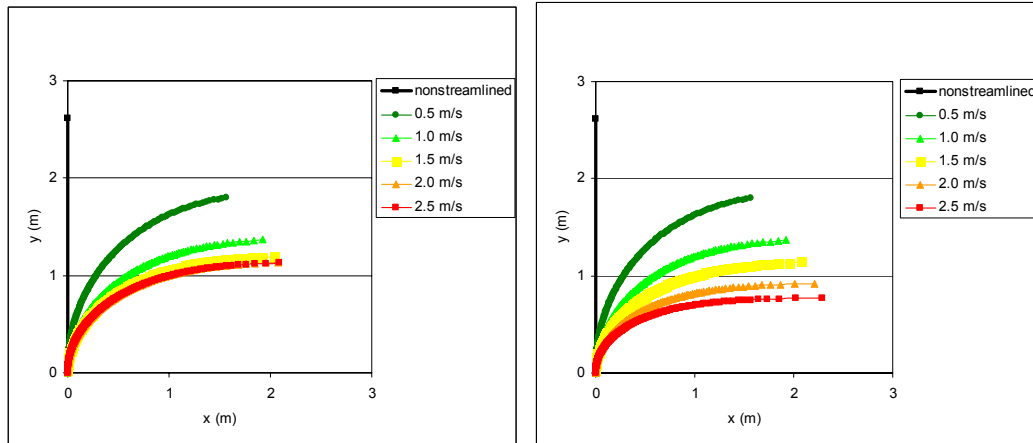
Figure II.10. Bending prediction for Las Vegas Wash Salt Cedar 4 resulting from "best fit" (a) and "maximum streamlining" (b) frontal area ratio assumptions.
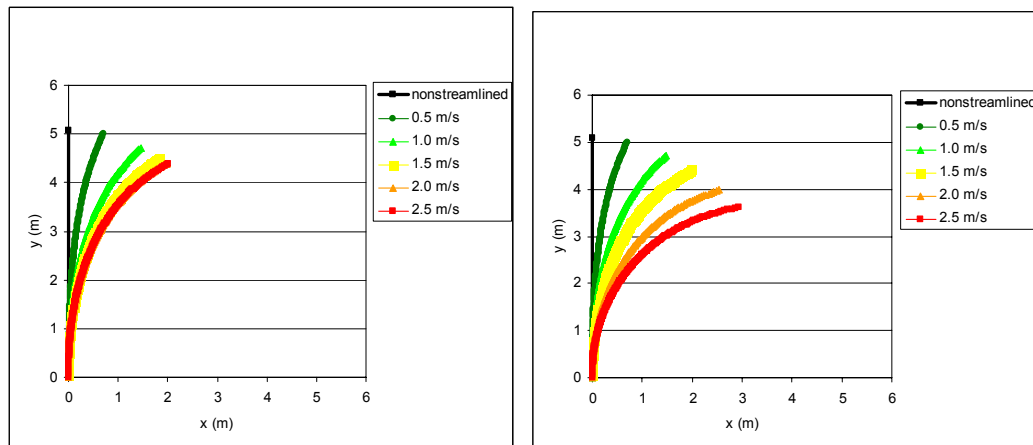
Figure II.11. Bending prediction for Las Vegas Wash Salt Cedar 9 resulting from "best fit" (a) and "maximum streamlining" (b) frontal area ratio assumptions.
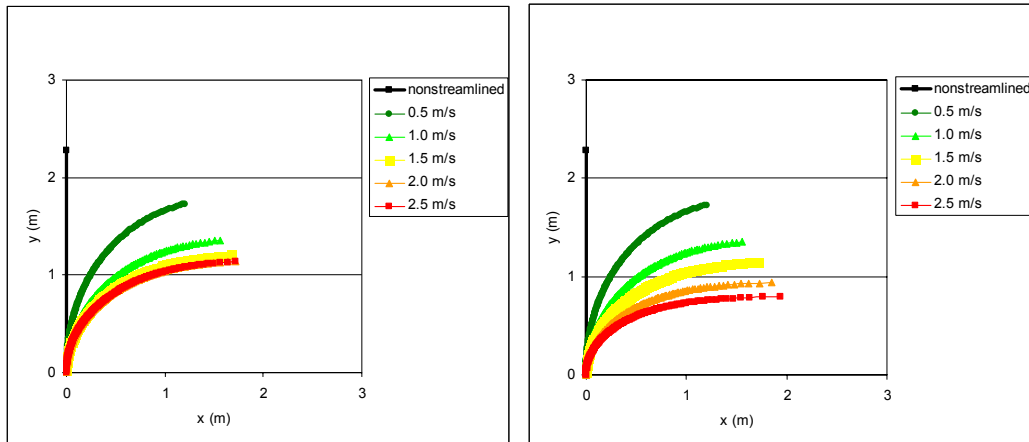
Figure II.12. Bending prediction for Las Vegas Wash Salt Cedar 13 resulting from "best fit" (a) and "maximum streamlining" (b) frontal area ratio assumptions.
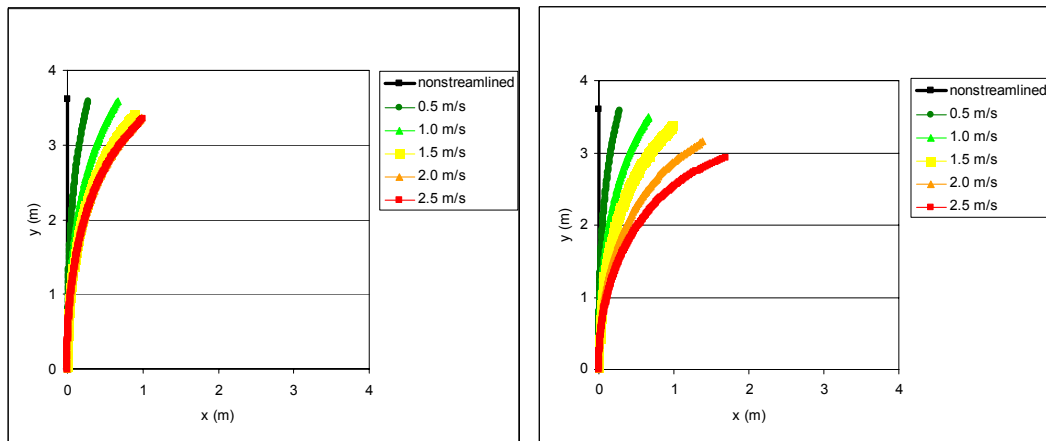
Figure II.13. Bending prediction for Rio Grande Salt Cedar 1 resulting from "best fit" (a) and "maximum streamlining" (b) frontal area ratio assumptions.
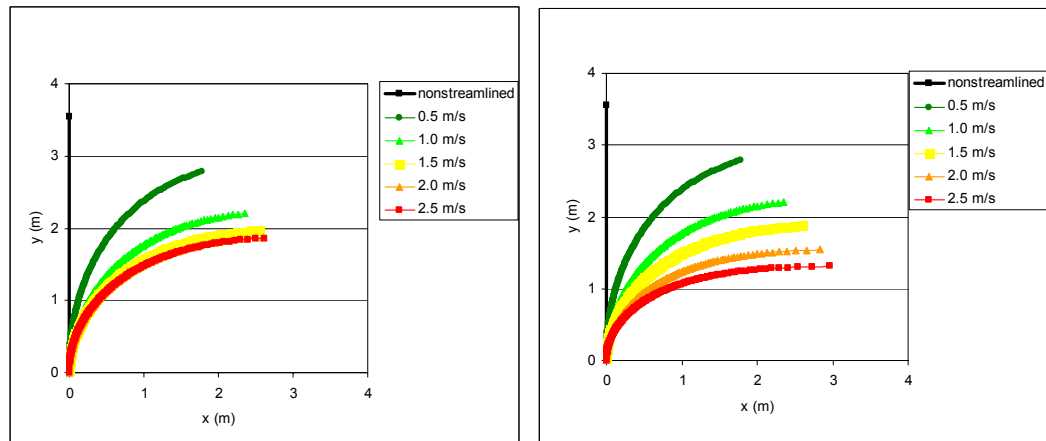
Figure II.14. Bending prediction for Rio Grande Salt Cedar 2 resulting from "best fit" (a) and "maximum streamlining" (b) frontal area ratio assumptions.

60
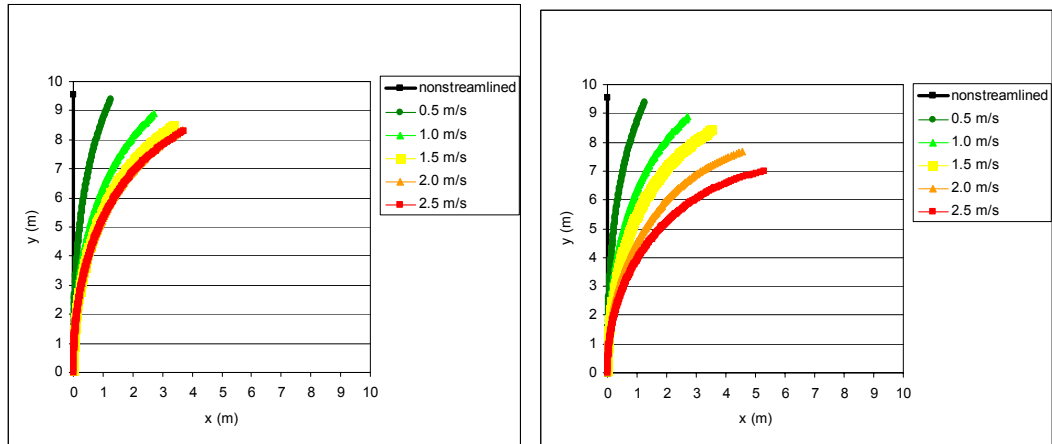
Figure II.15. Bending prediction for San Luis Rey Willow 10 resulting from "best fit" (a) and "maximum streamlining" (b) frontal area ratio assumptions.
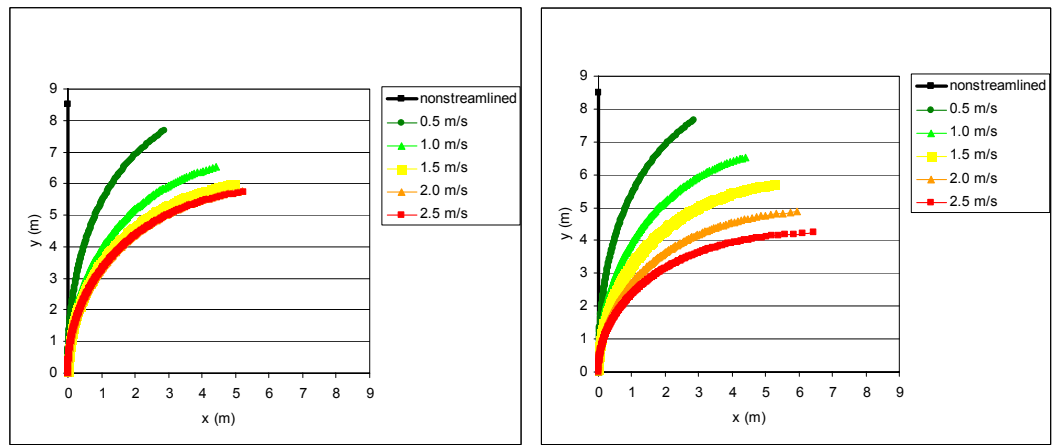
Figure II.16. Bending prediction for San Luis Rey Willow 9 resulting from "best fit" (a) and "maximum streamlining" (b) frontal area ratio assumptions.
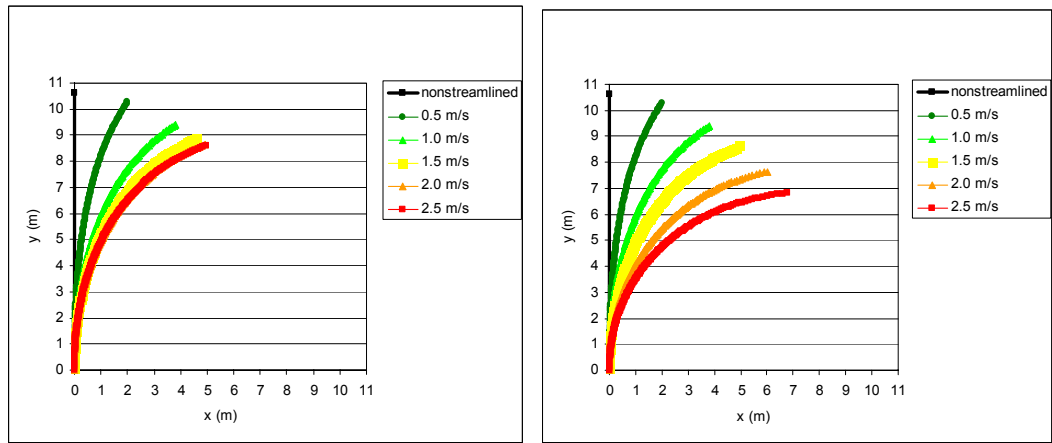
Figure II.17. Bending prediction for San Luis Rey Willow 8 resulting from "best fit" (a) and "maximum streamlining" (b) frontal area ratio assumptions.
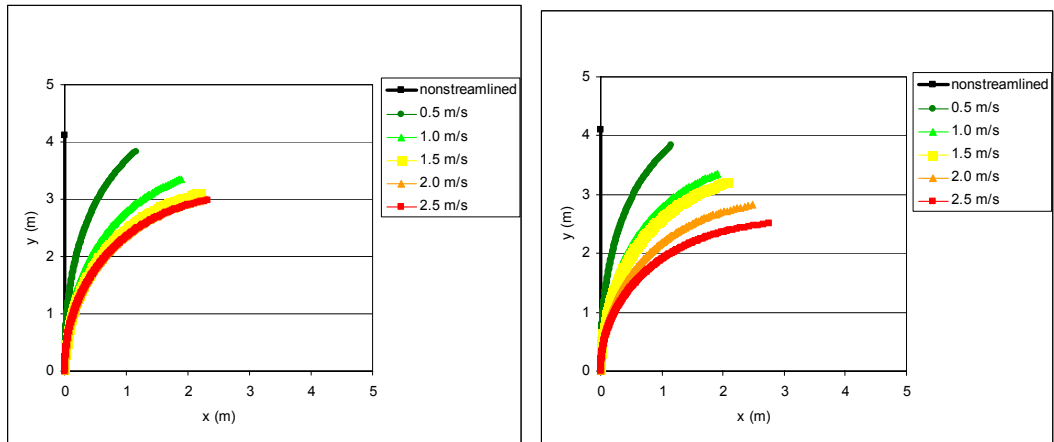
Figure II.18. Bending prediction for San Luis Rey Willow 7 resulting from "best fit" (a) and "maximum streamlining" (b) frontal area ratio assumptions.
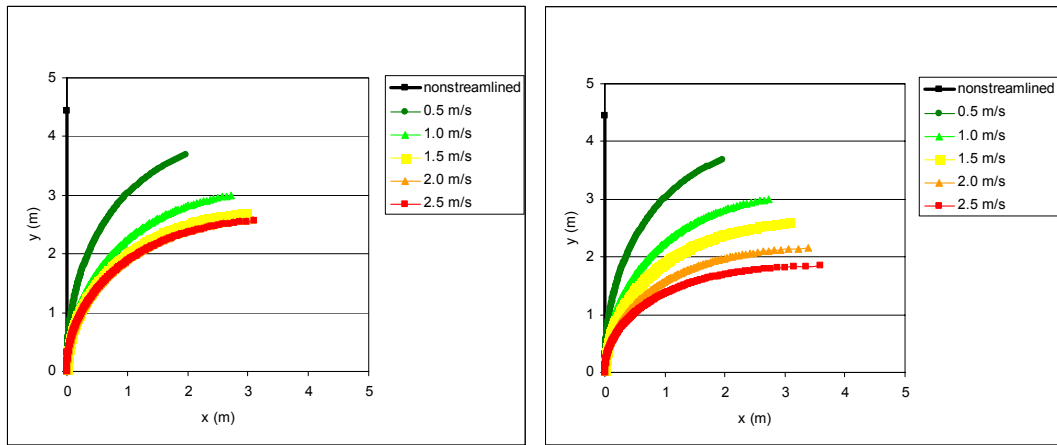
Figure II.19. Bending prediction for San Luis Rey Willow 6 resulting from "best fit" (a) and "maximum streamlining" (b) frontal area ratio assumptions.
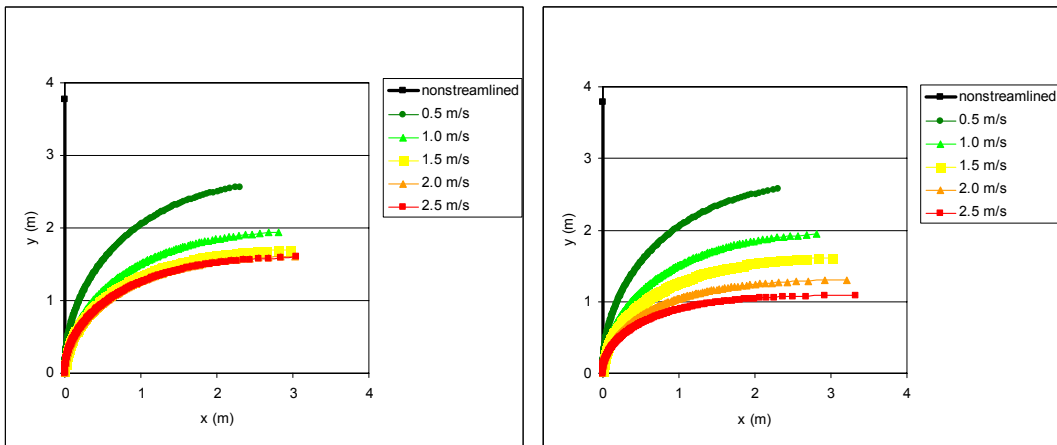
Figure II.20. Bending prediction for San Luis Rey Willow 5 resulting from "best fit" (a) and "maximum streamlining" (b) frontal area ratio assumptions.
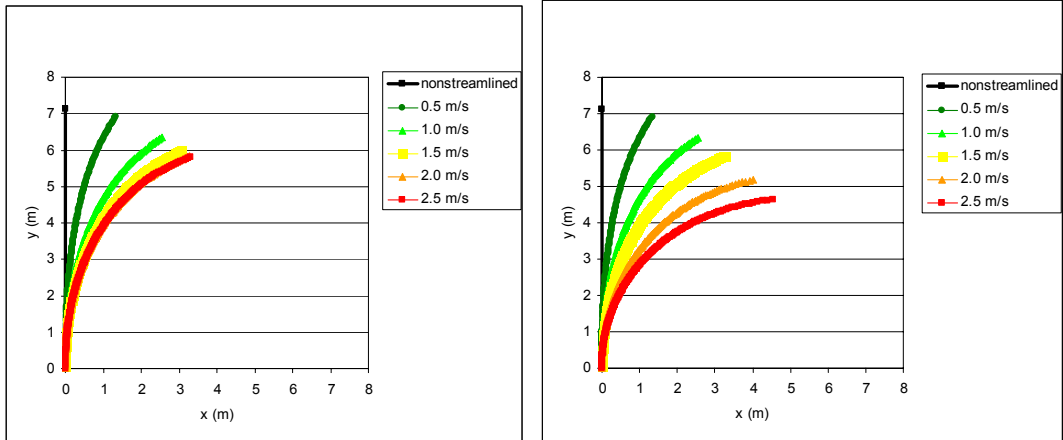
Figure II.21. Bending prediction for San Luis Rey Willow 4 resulting from "best fit" (a) and "maximum streamlining" (b) frontal area ratio assumptions.
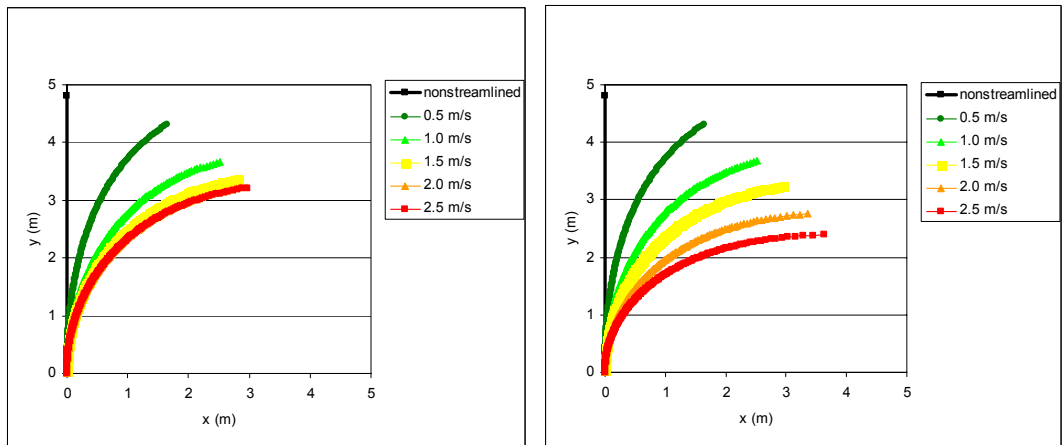
Figure II.22. Bending prediction for San Luis Rey Willow 3 resulting from "best fit" (a) and "maximum streamlining" (b) frontal area ratio assumptions.
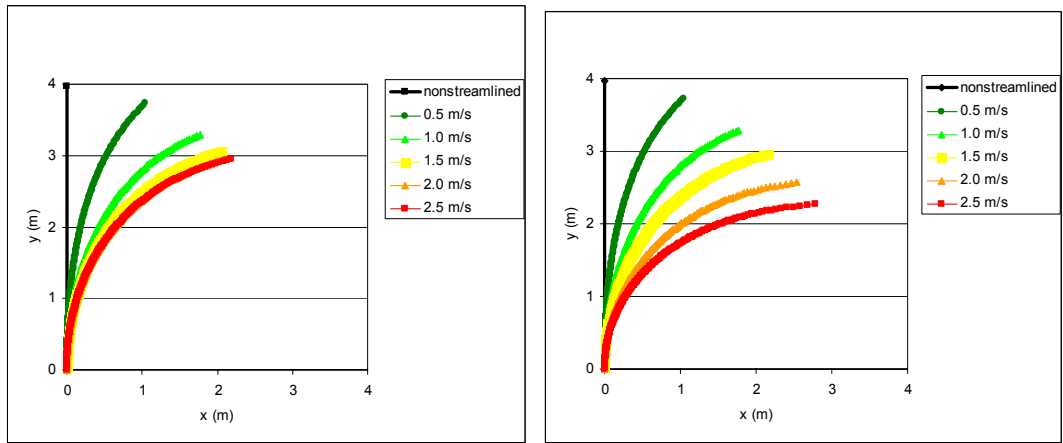
Figure II.23. Bending prediction for San Luis Rey Willow 2 resulting from "best fit" (a) and "maximum streamlining" (b) frontal area ratio assumptions.
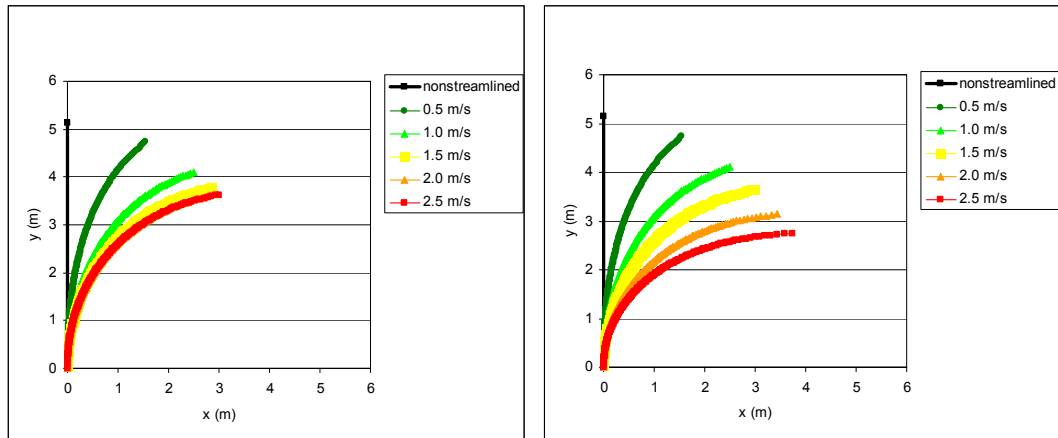
Figure II.24. Bending prediction for San Luis Rey Willow 1 resulting from "best fit" (a) and "maximum streamlining" (b) frontal area ratio assumptions.
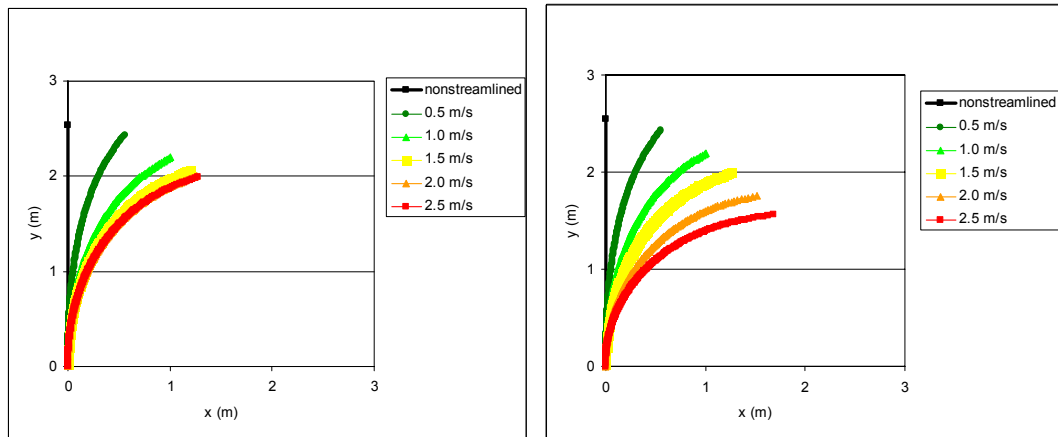
Figure II.25. Bending prediction for Rio Grande Willow 1 resulting from "best fit" (a) and "maximum streamlining" (b) frontal area ratio assumptions.
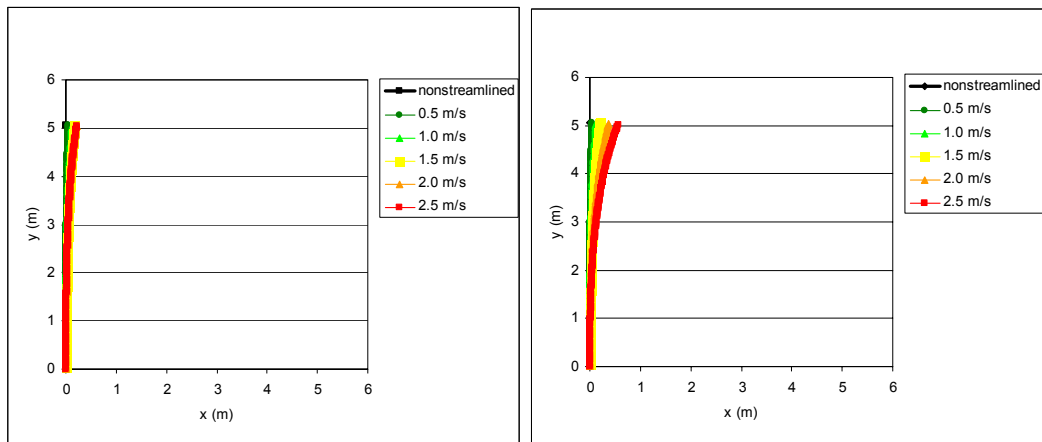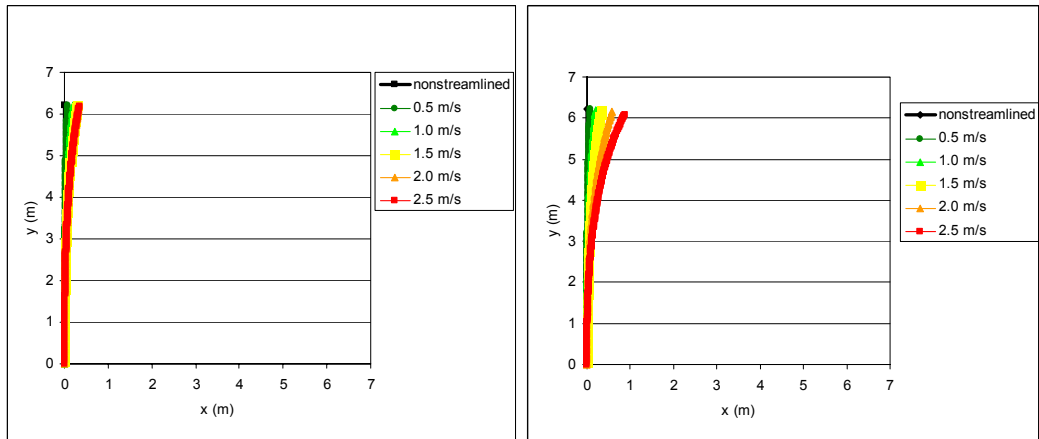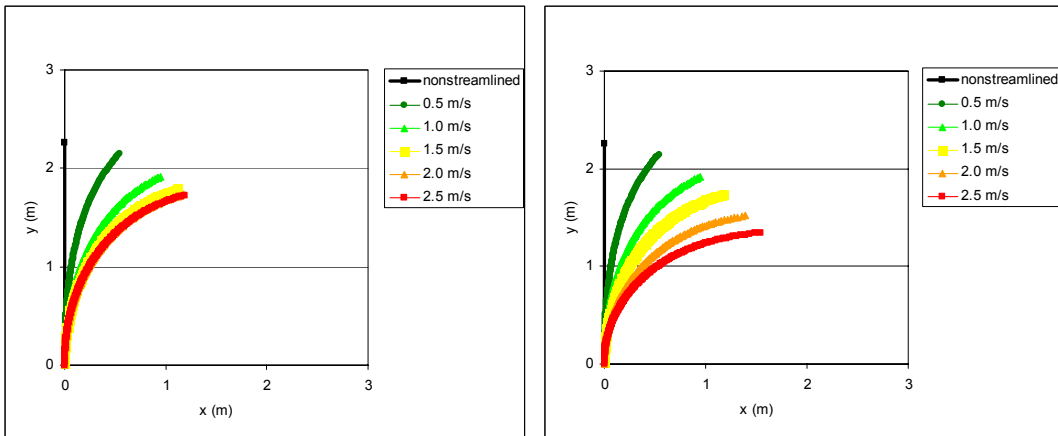

Figure II.26. Bending prediction for Rio Grande Willow 2 resulting from "best fit" (a) and "maximum streamlining" (b) frontal area ratio assumptions.

APPENDIX III

TREE BENDING PREDICTION TABLES

Table III.1. Bending prediction results derived from the "best fit" frontal area ratio
assumption.

Species	Tree ID	L (m)	Velocity (m/s)	F_d (N)	θ_{max}	β	l (m)	H_r
cottonwood	rg cw2	6.21	0.5	102.5	2.0	0.7	6.21	1.00
	rg cw1	5.06	0.5	40.5	1.5	0.5	5.06	1.00
	slr cw1	5.44	0.5	498.2	45.8	17.6	5.03	0.92
	slr cw3	7.48	0.5	402.9	32.2	11.7	7.22	0.97
	slr cw2	7.90	0.5	383.3	32.5	11.8	7.62	0.96
	slr cw4	2.12	0.5	55.0	75.9	38.8	1.52	0.72
cottonwood	rg cw2	6.21	1.0	268.9	5.3	1.8	6.21	1.00
	rg cw1	5.06	1.0	106.1	4.0	1.4	5.06	1.00
	slr cw1	5.44	1.0	1307.2	67.3	30.6	4.38	0.80
	slr cw3	7.48	1.0	1057.1	56.0	22.9	6.58	0.88
	slr cw2	7.90	1.0	1005.6	56.2	23.1	6.94	0.88
	slr cw4	2.12	1.0	144.4	84.6	52.6	1.17	0.55
cottonwood	rg cw2	6.21	1.5	396.9	7.7	2.7	6.20	1.00
	rg cw1	5.06	1.5	156.7	5.9	2.0	5.05	1.00
	slr cw1	5.44	1.5	1929.2	73.6	36.3	4.04	0.74
	slr cw3	7.48	1.5	1560.1	64.3	28.3	6.20	0.83
	slr cw2	7.90	1.5	1484.2	64.6	28.5	6.53	0.83
	slr cw4	2.12	1.5	213.1	86.4	57.6	1.03	0.48
cottonwood	rg cw2	6.21	2.0	462.8	9.0	3.1	6.19	1.00
	rg cw1	5.06	2.0	182.7	6.9	2.4	5.05	1.00
	slr cw1	5.44	2.0	2249.6	75.7	38.6	3.91	0.72
	slr cw3	7.48	2.0	1819.2	67.2	30.5	6.03	0.81
	slr cw2	7.90	2.0	1730.7	67.5	30.7	6.35	0.80
	slr cw4	2.12	2.0	248.5	87.0	59.5	0.98	0.46
cottonwood	rg cw2	6.21	2.5	474.3	9.2	3.2	6.19	1.00
	rg cw1	5.06	2.5	187.2	7.1	2.4	5.05	1.00
	slr cw1	5.44	2.5	2305.6	76.1	38.9	3.88	0.71
	slr cw3	7.48	2.5	1864.5	67.7	30.9	6.00	0.80
	slr cw2	7.90	2.5	1773.8	67.9	31.1	6.32	0.80
	slr cw4	2.12	2.5	254.7	87.1	59.8	0.97	0.46

Species	Tree ID	L (m)	Velocity (m/s)	F_d (N)	θ_{max}	β	l (m)	H_r
willow	slr wi10	9.54	0.5	662.6	21.6	7.7	9.40	0.99
	slr wi8	10.60	0.5	361.4	30.6	11.0	10.30	0.97
	slr wi4	7.13	0.5	352.9	30.3	10.9	6.90	0.97
	slr wi9	8.51	0.5	435.2	51.6	20.5	7.70	0.90
	slr wi3	4.80	0.5	149.1	52.2	20.9	4.30	0.90
	slr wi1	5.14	0.5	150.4	47.0	18.2	4.70	0.91
	rg wi1	2.54	0.5	25.0	35.2	12.9	2.40	0.94
	slr wi7	4.11	0.5	19.8	44.0	16.7	3.80	0.92

	rg wi2	2.26	0.5	13.5	38.2	14.2	2.10	0.93
	slr wi2	3.97	0.5	18.4	41.6	15.7	3.70	0.93
	slr wi6	4.44	0.5	34.1	64.0	28.1	3.70	0.83
	slr wi5	3.78	0.5	39.4	78.5	41.9	2.60	0.69
willow	slr wi10	9.54	1.0	1738.6	43.9	16.9	8.90	0.93
	slr wi8	10.60	1.0	948.1	54.4	22.0	9.40	0.89
	slr wi4	7.13	1.0	926.0	54.1	21.9	6.30	0.88
	slr wi9	8.51	1.0	1141.8	71.3	34.0	6.50	0.76
	slr wi3	4.80	1.0	391.2	71.7	34.4	3.70	0.77
	slr wi1	5.14	1.0	394.7	68.2	31.3	4.10	0.80
	rg wi1	2.54	1.0	65.7	58.8	24.6	2.20	0.87
	slr wi7	4.11	1.0	52.0	66.0	29.5	3.40	0.83
	rg wi2	2.26	1.0	35.3	61.4	26.3	1.90	0.84
	slr wi2	3.97	1.0	48.2	64.2	28.2	3.30	0.83
	slr wi6	4.44	1.0	89.6	78.7	42.2	3.00	0.68
	slr wi5	3.78	1.0	103.3	85.7	55.4	1.90	0.50
willow	slr wi10	9.54	1.5	2565.9	53.5	21.8	8.50	0.89
	slr wi8	10.60	1.5	1399.3	63.0	27.4	8.88	0.84
	slr wi4	7.13	1.5	1366.6	62.7	27.2	5.99	0.84
	slr wi9	8.51	1.5	1685.1	76.8	39.8	5.99	0.70
	slr wi3	4.80	1.5	577.4	77.1	40.1	3.36	0.70
	slr wi1	5.14	1.5	582.6	74.3	37.0	3.78	0.74
	rg wi1	2.54	1.5	96.9	66.7	30.1	2.06	0.81
	slr wi7	4.11	1.5	76.7	72.6	35.2	3.10	0.76
	rg wi2	2.26	1.5	52.1	68.8	31.8	1.79	0.79
	slr wi2	3.97	1.5	71.2	71.1	3.1	3.00	0.76
	slr wi6	4.44	1.5	132.2	82.3	47.8	2.70	0.61
	slr wi5	3.78	1.5	152.5	87.2	60.2	1.70	0.45
willow	slr wi10	9.54	2.0	2992.1	57.1	23.8	8.32	0.87
	slr wi8	10.60	2.0	1631.7	66.0	29.6	8.65	0.82
	slr wi4	7.13	2.0	1593.6	65.7	29.4	5.83	0.82
	slr wi9	8.51	2.0	1965.0	78.5	42.0	5.77	0.68
	slr wi3	4.80	2.0	673.3	78.8	42.4	3.23	0.67
	slr wi1	5.14	2.0	679.3	76.3	39.3	3.65	0.71
	rg wi1	2.54	2.0	113.0	69.4	32.3	2.00	0.79
	slr wi7	4.11	2.0	89.4	74.8	37.5	3.00	0.73
	rg wi2	2.26	2.0	60.7	71.4	34.1	1.74	0.77
	slr wi2	3.97	2.0	83.0	73.5	36.1	2.96	0.75
	slr wi6	4.44	2.0	154.2	83.4	50.0	2.58	0.58
	slr wi5	3.78	2.0	177.8	87.6	62.0	1.61	0.43
willow	slr wi10	9.54	2.5	3066.6	57.7	24.2	8.29	0.87
	slr wi8	10.60	2.5	1672.3	66.5	29.9	8.61	0.81
	slr wi4	7.13	2.5	1633.3	66.2	29.7	5.80	0.81
	slr wi9	8.51	2.5	2013.9	78.8	42.4	5.73	0.67
	slr wi3	4.80	2.5	690.1	79.1	42.7	3.21	0.67
	slr wi1	5.14	2.5	696.2	76.6	39.6	3.63	0.71
	rg wi1	2.54	2.5	115.8	69.8	32.7	1.99	0.78
	slr wi7	4.11	2.5	91.7	75.1	37.9	2.98	0.73

Species	Tree ID	L (m)	Velocity (m/s)	F$_d$ (N)	θ$_{max}$	β	l (m)	H$_r$
	rg wi2	2.26	2.5	62.3	71.8	34.5	1.73	0.76
	slr wi2	3.97	2.5	85.1	73.8	36.5	2.94	0.74
	slr wi6	4.44	2.5	158.0	83.6	50.3	2.57	0.58
	slr wi5	3.78	2.5	182.2	87.7	71.9	1.60	0.42

Species	Tree ID	L (m)	Velocity (m/s)	F$_d$ (N)	θ$_{max}$	β	l (m)	H$_r$
salt cedar	lvw sc9	5.08	0.5	930.6	22.7	8.0	5.00	0.98
	lvw sc2	3.45	0.5	259.2	15.0	5.2	3.42	0.99
	lvw sc1	4.71	0.5	287.0	73.0	35.6	3.54	0.75
	rg sc1	3.61	0.5	38.3	12.8	4.5	3.59	0.99
	slr sc1	2.99	0.5	175.6	76.0	38.9	2.58	0.86
	rg sc2	3.55	0.5	23.9	69.8	32.6	2.78	0.78
	lvw sc4	2.61	0.5	86.7	77.8	41.1	1.80	0.69
	lvw sc13	2.28	0.5	57.8	72.3	35.0	1.73	0.76
salt cedar	lvw sc9	5.08	1.0	2441.6	45.3	17.4	4.71	0.93
	lvw sc2	3.45	1.0	680.1	33.9	12.4	3.31	0.96
	lvw sc1	4.71	1.0	753.1	83.2	49.6	2.76	0.59
	rg sc1	3.61	1.0	100.6	29.9	10.8	3.50	0.97
	slr sc1	2.99	1.0	460.8	76.0	38.9	2.14	0.71
	rg sc2	3.55	1.0	62.8	81.7	46.8	2.21	0.62
	lvw sc4	2.61	1.0	227.4	85.4	54.6	1.37	0.52
	lvw sc13	2.28	1.0	151.5	82.9	49.0	1.36	0.59
salt cedar	lvw sc9	5.08	1.5	3603.4	54.9	22.3	4.50	0.89
	lvw sc2	3.45	1.5	1003.7	43.6	16.6	3.22	0.93
	lvw sc1	4.71	1.5	1111.5	85.5	54.9	2.45	0.52
	rg sc1	3.61	1.5	148.5	39.3	14.7	3.42	0.95
	slr sc1	2.99	1.5	680.1	80.3	44.6	1.94	0.65
	rg sc2	3.55	1.5	92.7	84.4	52.2	1.97	0.55
	lvw sc4	2.61	1.5	335.6	87.0	59.5	1.20	0.46
	lvw sc13	2.28	1.5	223.6	85.3	54.3	1.20	0.53
salt cedar	lvw sc9	5.08	2.0	4201.9	58.4	24.4	4.40	0.87
	lvw sc2	3.45	2.0	1170.4	47.5	18.4	3.17	0.92
	lvw sc1	4.71	2.0	1296.1	86.2	56.9	2.33	0.50
	rg sc1	3.61	2.0	173.1	43.2	16.4	3.37	0.93
	slr sc1	2.99	2.0	793.0	81.7	46.8	1.86	0.62
	rg sc2	3.55	2.0	108.1	85.2	54.2	1.88	0.53
	lvw sc4	2.61	2.0	391.4	87.4	61.3	1.14	0.44
	lvw sc13	2.28	2.0	260.8	86.0	56.3	1.14	0.50
salt cedar	lvw sc9	5.08	2.5	4306.5	58.9	24.7	4.39	0.86
	lvw sc2	3.45	2.5	1199.5	48.1	18.7	3.16	0.92
	lvw sc1	4.71	2.5	1328.4	86.3	57.2	2.31	0.49
	rg sc1	3.61	2.5	177.4	43.9	16.7	3.37	0.93
	slr sc1	2.99	2.5	812.8	81.9	47.1	1.85	0.62
	rg sc2	3.55	2.5	110.8	85.4	54.6	1.86	0.52
	lvw sc4	2.61	2.5	401.1	87.5	61.6	1.13	0.43
	lvw sc13	2.28	2.5	267.3	86.1	56.6	1.14	0.50

Table III.2. Bending prediction results derived from the "maximum streamlining" frontal area ratio assumption.

Species	Tree ID	L (m)	Velocity (m/s)	F_d (N)	θ_{max}	β	l (m)	H_r
cottonwood	rg cw2	6.21	0.5	102.5	2.0	0.7	6.21	1.00
	rg cw1	5.06	0.5	40.5	1.5	0.5	5.06	1.00
	slr cw1	5.44	0.5	498.2	45.8	17.6	5.03	0.92
	slr cw3	7.48	0.5	402.9	32.2	11.7	7.22	0.97
	slr cw2	7.90	0.5	383.3	32.5	11.8	7.62	0.96
	slr cw4	2.12	0.5	55.0	75.9	38.8	1.52	0.72
cottonwood	rg cw2	6.21	1.0	268.9	5.3	1.8	6.21	1.00
	rg cw1	5.06	1.0	106.1	4.0	1.4	5.06	1.00
	slr cw1	5.44	1.0	1307.2	67.3	30.6	4.38	0.80
	slr cw3	7.48	1.0	1057.1	56.0	22.9	6.58	0.88
	slr cw2	7.90	1.0	1005.6	56.2	23.1	6.94	0.88
	slr cw4	2.12	1.0	144.4	84.6	52.6	1.17	0.55
cottonwood	rg cw2	6.21	1.5	461.9	9.0	3.1	6.19	1.00
	rg cw1	5.06	1.5	182.3	6.9	2.4	5.05	1.00
	slr cw1	5.44	1.5	2245.2	75.7	38.5	3.91	0.72
	slr cw3	7.48	1.5	1815.7	67.2	30.5	6.03	0.81
	slr cw2	7.90	1.5	1727.3	67.4	30.7	6.35	0.80
	slr cw4	2.12	1.5	248.1	87.0	59.5	0.98	0.46
cottonwood	rg cw2	6.21	2.0	821.2	15.6	5.4	6.16	0.99
	rg cw1	5.06	2.0	324.1	12.0	4.2	5.04	1.00
	slr cw1	5.44	2.0	3991.4	81.8	46.9	3.37	0.62
	slr cw3	7.48	2.0	3227.9	76.1	39.0	5.34	0.71
	slr cw2	7.90	2.0	3070.8	76.2	39.1	5.62	0.71
	slr cw4	2.12	2.0	441.0	88.4	65.9	0.79	0.37
cottonwood	rg cw2	6.21	2.5	1283.1	23.2	8.2	6.10	0.98
	rg cw1	5.06	2.5	506.5	18.2	6.4	5.01	0.99
	slr cw1	5.44	2.5	6236.6	84.8	53.1	2.95	0.54
	slr cw3	7.48	2.5	5043.6	80.9	45.5	4.77	0.64
	slr cw2	7.90	2.5	4798.1	81.0	45.7	5.02	0.63
	slr cw4	2.12	2.5	689.0	89.0	70.1	0.67	0.31

Species	Tree ID	L (m)	Velocity (m/s)	F_d (N)	θ_{max}	β	l (m)	H_r
willow	slr wi10	9.54	0.5	662.6	21.6	7.7	9.40	0.99
	slr wi8	10.60	0.5	361.4	30.6	11.0	10.30	0.97
	slr wi4	7.13	0.5	352.9	30.3	10.9	6.90	0.97
	slr wi9	8.51	0.5	435.2	51.6	20.5	7.70	0.90
	slr wi3	4.80	0.5	149.1	52.2	20.9	4.30	0.90
	slr wi1	5.14	0.5	150.4	47.0	18.2	4.70	0.91
	rg wi1	2.54	0.5	25.0	35.2	12.9	2.40	0.94
	slr wi7	4.11	0.5	19.8	44.0	16.7	3.80	0.92
	rg wi2	2.26	0.5	13.5	38.2	14.2	2.10	0.93
	slr wi2	3.97	0.5	18.4	41.6	15.7	3.70	0.93
	slr wi6	4.44	0.5	34.1	64.0	28.1	3.70	0.83
	slr wi5	3.78	0.5	39.4	78.5	41.9	2.60	0.69

willow	slr wi10	9.54	1.0	1738.6	43.9	16.9	8.90	0.93
	slr wi8	10.60	1.0	948.1	54.4	22.0	9.40	0.89
	slr wi4	7.13	1.0	926.0	54.1	21.9	6.30	0.88
	slr wi9	8.51	1.0	1141.8	71.3	34.0	6.50	0.76
	slr wi3	4.80	1.0	391.2	71.7	34.4	3.70	0.77
	slr wi1	5.14	1.0	394.7	68.2	31.3	4.10	0.80
	rg wi1	2.54	1.0	65.7	58.8	24.6	2.20	0.87
	slr wi7	4.11	1.0	52.0	66.0	29.5	3.40	0.83
	rg wi2	2.26	1.0	35.3	61.4	26.3	1.90	0.84
	slr wi2	3.97	1.0	48.2	64.2	28.2	3.30	0.83
	slr wi6	4.44	1.0	89.6	78.7	42.2	3.00	0.68
	slr wi5	3.78	1.0	103.3	85.7	55.4	1.90	0.50
willow	slr wi10	9.54	1.5	2986.2	55.3	22.6	8.40	0.88
	slr wi8	10.60	1.5	1628.5	66.3	29.8	8.60	0.81
	slr wi4	7.13	1.5	1590.5	65.7	29.3	5.80	0.81
	slr wi9	8.51	1.5	1961.1	78.8	42.5	5.70	0.67
	slr wi3	4.80	1.5	672.0	78.8	42.4	3.20	0.67
	slr wi1	5.14	1.5	678.0	76.3	39.2	3.70	0.72
	rg wi1	2.54	1.5	112.8	69.4	32.3	2.00	0.79
	slr wi7	4.11	1.5	89.3	70.0	32.9	3.20	0.78
	rg wi2	2.26	1.5	60.6	71.4	34.1	1.70	0.75
	slr wi2	3.97	1.5	82.8	73.4	36.1	3.00	0.76
	slr wi6	4.44	1.5	153.9	83.4	50.0	2.60	0.59
	slr wi5	3.78	1.5	177.4	87.6	62.0	1.60	0.42
willow	slr wi10	9.54	2.0	5308.9	67.3	30.6	7.70	0.81
	slr wi8	10.60	2.0	2895.1	75.5	38.2	7.60	0.72
	slr wi4	7.13	2.0	2827.6	75.0	37.8	5.20	0.73
	slr wi9	8.51	2.0	3486.5	83.7	50.7	4.90	0.58
	slr wi3	4.80	2.0	1194.7	83.7	50.6	2.80	0.58
	slr wi1	5.14	2.0	1205.3	82.1	47.6	3.10	0.60
	rg wi1	2.54	2.0	200.6	77.6	40.8	1.80	0.71
	slr wi7	4.11	2.0	158.7	78.0	41.3	2.80	0.68
	rg wi2	2.26	2.0	107.8	78.9	42.5	1.50	0.66
	slr wi2	3.97	2.0	147.3	80.3	44.5	2.60	0.65
	slr wi6	4.44	2.0	273.6	86.4	57.6	2.20	0.50
	slr wi5	3.78	2.0	315.4	88.7	68.0	1.30	0.34
willow	slr wi10	9.54	2.5	8295.1	74.5	37.1	7.00	0.73
	slr wi8	10.60	2.5	4523.5	80.4	44.8	6.80	0.64
	slr wi4	7.13	2.5	4418.1	80.1	44.3	4.60	0.65
	slr wi9	8.51	2.5	5447.6	86.1	56.6	4.20	0.49
	slr wi3	4.80	2.5	1866.7	86.1	56.5	2.40	0.50
	slr wi1	5.14	2.5	1883.3	85.1	53.8	2.70	0.53
	rg wi1	2.54	2.5	313.4	81.9	47.3	1.60	0.63
	slr wi7	4.11	2.5	248.0	82.2	47.8	2.50	0.61
	rg wi2	2.26	2.5	168.4	82.9	49.0	1.30	0.58
	slr wi2	3.97	2.5	230.1	83.8	50.9	2.30	0.58
	slr wi6	4.44	2.5	427.5	87.8	62.8	1.80	0.41
	slr wi5	3.78	2.5	492.9	89.2	71.9	1.10	0.29

Species	Tree ID	L (m)	Velocity (m/s)	F_d (N)	θ_{max}	β	l (m)	H_r
salt cedar	lvw sc9	5.08	0.5	930.6	22.7	8.0	5.00	0.98
	lvw sc2	3.45	0.5	259.2	15.0	5.2	3.42	0.99
	lvw sc1	4.71	0.5	287.0	73.0	35.6	3.54	0.75
	rg sc1	3.61	0.5	38.3	12.8	4.5	3.59	0.99
	slr sc1	2.99	0.5	175.6	76.0	38.9	2.58	0.86
	rg sc2	3.55	0.5	23.9	69.8	32.6	2.78	0.78
	lvw sc4	2.61	0.5	86.7	77.8	41.1	1.80	0.69
	lvw sc13	2.28	0.5	57.8	72.3	35.0	1.73	0.76
salt cedar	lvw sc9	5.08	1.0	2441.6	45.3	17.4	4.71	0.93
	lvw sc2	3.45	1.0	680.1	33.9	12.4	3.31	0.96
	lvw sc1	4.71	1.0	753.1	83.2	49.6	2.76	0.59
	rg sc1	3.61	1.0	100.6	29.9	10.8	3.50	0.97
	slr sc1	2.99	1.0	460.8	76.0	38.9	2.14	0.71
	rg sc2	3.55	1.0	62.8	81.7	46.8	2.21	0.62
	lvw sc4	2.61	1.0	227.4	85.4	54.6	1.37	0.52
	lvw sc13	2.28	1.0	151.5	82.9	49.0	1.36	0.59
salt cedar	lvw sc9	5.08	1.5	4193.7	58.3	24.3	4.41	0.87
	lvw sc2	3.45	1.5	1168.1	47.4	18.4	3.17	0.92
	lvw sc1	4.71	1.5	1293.6	86.2	56.8	2.33	0.50
	rg sc1	3.61	1.5	172.8	43.2	16.4	3.37	0.93
	slr sc1	2.99	1.5	791.5	81.7	46.7	1.86	0.62
	rg sc2	3.55	1.5	107.9	85.2	54.2	1.88	0.53
	lvw sc4	2.61	1.5	390.6	87.4	61.3	1.14	0.44
	lvw sc13	2.28	1.5	260.3	86.0	56.3	1.15	0.50
salt cedar	lvw sc9	5.08	2.0	7455.4	69.6	32.5	3.99	0.78
	lvw sc2	3.45	2.0	2076.6	60.9	26.0	2.93	0.85
	lvw sc1	4.71	2.0	2299.7	88.0	63.6	1.91	0.41
	rg sc1	3.61	2.0	307.2	57.2	23.7	3.15	0.87
	slr sc1	2.99	2.0	1407.1	85.4	54.7	1.56	0.52
	rg sc2	3.55	2.0	191.9	87.4	61.3	1.55	0.44
	lvw sc4	2.61	2.0	694.5	88.6	67.4	0.92	0.35
	lvw sc13	2.28	2.0	462.7	87.9	63.1	0.94	0.41
salt cedar	lvw sc9	5.08	2.5	11649.1	76.2	39.1	3.62	0.71
	lvw sc2	3.45	2.5	3244.8	69.5	32.4	2.71	0.79
	lvw sc1	4.71	2.5	3593.3	88.8	68.1	1.61	0.34
	rg sc1	3.61	2.5	479.9	66.5	29.9	2.93	0.81
	slr sc1	2.99	2.5	2198.5	87.2	60.2	1.35	0.45
	rg sc2	3.55	2.5	299.8	88.4	66..2	1.31	0.37
	lvw sc4	2.61	2.5	1085.1	89.2	71.4	0.77	0.30
	lvw sc13	2.28	2.5	723.0	88.7	67.7	0.79	0.35

APPENDIX IV

TREE BENDING PREDICTIVE ALGORITHM

Under the assumption that the material of beam remains linearly elastic, the

relationship of bending moment and beam deformation is given by

$$\frac{\dfrac{d^2x}{dy^2}}{\left[1+\left(\dfrac{dx}{dy}\right)^2\right]^{\frac{3}{2}}} = \frac{M(y)}{EI} \tag{1}$$

where θ is the angle of rotation of the deflection curve, θ_m is θ at the free end, s is the

distance measured along the beam, x and y are coordinates in which y is parallel to the

original beam, E is the modulus of elasticity of the material and I is the moment of inertia

of the cross-sectional area of the beam about the axis of bending. Its solution, $x = f(y)$,

gives the exact shape of the elastic curve.

Ang Jr. et al. (1993) proposed a numerical method applying a search procedure to

solve this problem. With

$$z = \frac{dx}{dy} \tag{2}$$

the curve length of the beam can be calculated with

$$s(l) = \int_0^l \sqrt{1+\left(\frac{dx}{dy}\right)^2}\, dy \tag{3}$$

and

$$\frac{ds}{dy} = \sqrt{1 + z^2}$$ (4)

Equation 1 can then be converted to

$$\frac{dz}{dy} = \frac{M(y)}{EI}\left(1 + z^2\right)^{3/2}$$ (5)

where

$$M(y) = \frac{F_d}{2l}\left(2ly - y^2 - l^2\right)$$ (6)

Equations 2, 4 and 5 can be numerically solved for a given projective length l with boundary conditions $z(0) = x(0) = s(0) = 0$ at the fixed end. The problem will then be solved by searching the projective length l until

$$s(l) = L$$ (7)

Chen (2009) proposed a new approach to solve the cantilever beam problem based on the formulation by Ang Jr. et al (1993). Equation 5 is rewritten into

$$\frac{dz}{\left(1+z^2\right)^{3/2}} = \frac{M(y)}{EI}dy \qquad (8)$$

Using the boundary condition $z(0) = 0$, Equation 8 can then be integrated to give

$$\frac{z}{\sqrt{1+z^2}} = \int_0^y \frac{M(y)}{EI}dy = Q(y) - Q(0) = G(y) \qquad (9)$$

Using equation 4, the above equation can be converted to

$$\frac{ds}{dy} = \frac{1}{\sqrt{1-G^2(y)}} \qquad (10)$$

From Equation 2, another equation for variable x can be obtained following the same procedure, which reads

$$\frac{dx}{dy} = \frac{G(y)}{\sqrt{1-G^2(y)}} \qquad (11)$$

Equations 10 and 11 become the new governing equations for the large deflection cantilever beam bending problem. For simple load and uniform beam cases, can be solved following the search procedure. With a given l value, the function $G(y)$ can be determined analytically or numerically through integration of the bending moment as defined in Equation 9. Once the function $G(y)$ is determined, Equation 10 can be integrated with respect to y from 0 to l to find the arc length $s(l)$. If $s(l) \neq L$, a new l value will be assumed according to the calculated $s(l)$ value and the search procedure can be repeated until the correct l is found.

DATALOGGER PROGRAM

AND EQUIPMENT LIST

```
'CR1000 Series Datalogger
'date: June 16, 2008
'program author: John Goreham
'program to read BOTH a 2,000 lb and a 10,000 lb capacity strain gage

'SET FLAG 1 HIGH TO RECORD MEASUREMENTS

'Declare Public Variables
Public PTemp,batt_volt,Flag
Public response2000, response10000, lb_force2000, lb_force10000
Public h_response, v_response, h_angle, v_angle
Public period,VWC

'Define Data Tables
DataTable (Table1,1,-1)
        DataInterval (0,1,Sec,10)
        Sample (1,PTemp,FP2)
        Sample (1,batt_volt,FP2)
        Sample (1,response2000,FP2)
        Sample (1,lb_force2000,FP2)
        Sample (1,response10000,FP2)
        Sample (1,lb_force10000,FP2)
        Sample (1,v_angle,FP2)
        Sample (1,h_angle,FP2)
        Sample (1,period,FP2)
        Sample (1,VWC,FP2)
EndTable

'Main Program
BeginProg
        Scan (1,Sec,0,0)
                PanelTemp (PTemp,250)
                Battery (batt_volt)

                VoltDiff (response2000,1,mV25,1,True ,0,250,1.0,0)
                lb_force2000=response2000*66.599-0.0289
                VoltDiff (response10000,1,mV25,2,True ,0,250,1.0,0)
                lb_force10000=response10000*333.24-1.4291
```

```
VoltSe (v_response,1,mV5000,7,1,0,250,1.0,0)
v_angle=0.06*v_response-150
VoltSe (h_response,1,mV5000,8,1,0,250,1.0,0)
h_angle=0.06*h_response-150

CS616 (period,1,5,1,1,1.0,0)
VWC=-0.4677+0.0283*period

If Flag<>0 Then
        CallTable (Table1)
EndIf
NextScan
EndProg
```

Item	Vendor	Model
cr 1000 datalogger	campbell scientific	
ps 100-SW 12 Vdc power supply	campbell scientific	
wall charger 18 Vac 1.2A	campbell scientific	9591
SC32B optically isolated RS-232 interface	campbell scientific	
CS616 water content reflectometer	campbell scientific	
vertical inclinometer	spectron sensors	SSY0185-VRS
horizontal inclinometer	spectron sensors	SSY0185-HRS
breadboard	digikey	438-1045-ND
IC REGULATOR 3PIN 10V TO220FP	digikey	BA17810T-ND
white poly tarp for photo background 15' x 20'	tarps plus	
ENVIRONMENT PROTECTED LOADCELL	omega	LCCD-2K
MALE ROD END THREAD 1/2-20	omega	REC-012M
ENVIRONMENT PROTECTED LOADCELLPR	omega	LCCD-10K
MALE ROD END THREAD 3/4-16	omega	REC-034M
5/16" anchor shackles	mcmaster	3797T44
5/8" shackles with hitch pin	mcmaster	3780T11
long nylon sling	mcmaster	3383T218
sling hook	mcmaster	8864T654
calipers	forestry suppliers	59734
peltor lumberjack hardhat	forestry suppliers	24433
pulley block	northern tool	141213
WARN® RT40 12V DC ATV Winch	northern tool	RT 40
winch mount	northern tool	147015

rubber wheel blocks	mcmaster	2232T14
deka marine master & RV heavy duty deep cycle		

Figure VI.1. Winch used for tree pulling field experiments. The winch was powered by the deep cycle marine batteries located in the truck bed. The black toolbox on the right side of the tailgate houses a CR1000 datalogger. A laptop computer connected to the datalogger enabled real-time monitoring of experimental data.

Figure VI. 2. Digital photograph of a San Luis Rey salt cedar used for determination of nonstreamlined frontal area (A_0) and height (L). Note the yellow yardstick located to the lower right of the tree for image scaling.

Figure VI. 3. Strain gauge and horizontal inclinometer. The apparatus was attached to the winch pull line and measured both the force applied to the tree and the angle of the pull line.

Figure VI. 4. Preparation of the tree pulling apparatus prior to testing conducted on a Rio Grande cottonwood. Note the vertical inclinometer attached to the tree near the winch line attachment on the tree trunk. The strain gauge/horizontal inclinometer apparatus pictured in Figure VI.3 above can be seen hanging from the winch line near the researchers.

Figure VI. 5. Photo taken during a pull test conducted on a Rio Grande cottonwood. The strain gauge/horizontal inclinometer apparatus pictured in Figure VI.3 above can be seen toward the left center edge of the image hanging from the winch line.

REFERENCES

Ang Jr., M.H., Wang, W., and Low, T.S., 1993. On the estimation of the large deflection of a cantilever beam. Proceedings of the IEEE IES Annual Conference, IECON'93, Hawaii, USA, November 1993, pp1604-1609.

Baptist, M.J., Babovic, V., Rodriguez-Uthurburu, J., Keijzer, M., Mynett, A., and Verwey, A., 2007. On Inducing Equations for Vegetation Resistance. Journal of Hydraulic Research, International Association of Hydraulic Engineering and Research, Vol. 45 (4), pp. 435-450.

Coutts, M.P., 1983. Root Architecture and Tree Stability. Plant and Soil, Vol. 71, pp. 171-188.

Fischenich, J.C., 2000. Resistance Due to Vegetation. ERDC TN-EMRRP-SR-07. Engineer Research and Development Center, Vicksburg, Mississippi.

Freeman, G.E., Rahmeyer, W.H., and Copeland, R.R., 2000. Determination of Resistance Due to Shrubs and Woody Vegetation. ERDC/CHL TR-00-25. U.S. Army Engineer Research and Development Center, Vicksburg, Mississippi.

Gardiner, B., Byrne, K., Hale, S., Kamimura, K., Mitchell, S.J., Peltola, H., Ruel, J-C., 2008. A Review of Mechanistic Modelling of Wind Damage Risk to Forests. Forestry, 81 (3), 447-463.

Hibbeler, R. C., 2009. Structural Analysis, Prentice-Hall Inc., Upper Saddle River, New Jersey.

Jarvela, J., 2004. Determination of Flow Resistance Caused by Non-Submerged Woody Vegetation. International Journal of River Basin Management. IAHR, Vol. 2 (1).

James, K. R., Haritos, N., Ades, P. K., 2006. Mechanical Stability of Trees Under Dynamic Loads. Am. J. Bot. 2006 93: 1522-1530.

Kane, B., Smiley, E.T., 2006. Drag Coefficients and Crown Area Estimation of Red Maple. Canadian Journal of Forest Research, 36(8): 1951-1958.

Kouwen, N., Li, R.M., and Simons, D.B., 1981. Flow Resistance in Vegetated Waterways. Transactions of the ASAE. ASAE, Vol. 24 (3).

Lopez, F., and Garcia, M.H., 2001. Mean Flow and Turbulence Structure of Open Channel Flow Through Non-Emergent Vegetation. Journal of Hydraulic Engineering. ASCE, Vol. 127 (5).

Lundström, T., Jonas, T., Stöckli, V., and Ammann, W., 2007. Anchorage of Mature Conifers: Resistive Turning Moment, Root-Soil Plate Geometry and Root Growth Orientation. Tree Physiology. Heron, Vol. 27 (9), pp.1217-27.

Nepf, H.M., 1999. Drag, Turbulence, and Diffusion in Flow Through Emergent Vegetation. Water Resources Research. AGU, Vol. 35 (2).

Nicoll, B.C., Gardiner, B.A., Rayner, B., and Peace, A.J., 2006. Anchorage of Coniferous Tress in Relation to Species, Soil Type, and Rooting Depth. Canadian Journal of Forest Research. NRC Canada, Vol. 36 (7), pp. 1871-1883.

Norris, J.E., Stokes, A., Mickovski, S.B., Cammeraat, E., van Beek, R., Nicoll, B.C., and Achim, A., 2008. Slope Stability and Erosion Control: Ecotechnological Solutions. Springer, Dordrecht, The Netherlands.

Peltola, H.M., 2006. Mechanical Stability of Trees Under Static Loads. American Journal of Botany. Botanical Society of America, Vol. 93 (10), pp. 1501-1511.

Petryk, S., and Bosmajian, G., 1975. Analysis of Flow Through Vegetation. Journal of the Hydraulics Division. ASCE, Vol. 101 (HY7).

Rudnicki, M., Mitchell, S.J., and Novak, M.D., 2004. Wind Tunnel Measurements of Crown Streamlining and Drag Relationships for Three Conifer Species. Can. J. For. Res. 34: 666–676.

Wilson, C.A.M.E., Hoyt, J., and Schnauder, I., 2008. Impact of Foilage on the Drag Force of Vegetation in Aquatic Flows. Journal of Hydraulic Engineering. ASCE, Vol. 134 (7), pp. 885-891.

Wilson, C.A.M.E., Stoesser, T., Bates, P.D., and Pinzen, A.B., 2003. Open Channel Flow Through Different Forms of Submerged Flexible Vegetation. Journal of Hydraulic Engineering. ASCE, Vol. 129 (11), pp. 847-853.

Vollsinger, S., Mitchell, S.J., Byrne, K.E., Novak, M.D., and Rudnicki, M., 2005. Wind Tunnel Measurements of Crown Streamlining and Drag Relationships for Several Hardwood Species. Canadian Journal of Forest Research, Vol. 35, pp. 1238-1249.

Yen, B.C., 2002. Open Channel Flow Resistance. Journal of Hydraulic Engineering. American Society of Civil Engineers, Vol. 128 (1), pp. 20-39.

VITA

Graduate College
University of Nevada, Las Vegas

John O. Goreham

Home Address:
    2671 South Decatur Boulevard #1116
    Las Vegas, NV 89102

Degrees:
    Bachelor of Science, Agriculture, 2001
    New Mexico State University, Las Cruces

Thesis Title:
    Bending of Woody Riparian Vegetation as a Function of Hydraulic Flow Conditions

Thesis Examination Committee:
    Chairperson, Dr. Zhongbo Yu, Ph. D.
    Co-Chairperson, Dr. Mark Stone, Ph. D.
    Committee member, Dr. Kumud Acharya, Ph. D.
    Graduate Faculty Representative, Dr. Robert Futrell, Ph. D.